Memoirs of the School of Engineering, Nagoya University
Vol.44. No.2 (1992)

SECOND-ORDER WAVE EFFECTS ON OCEAN PLATFORMS: THEORY AND EXPERIMENT

Tetsuya MATSUI

Department of Architecture

(Received November 2, 1992)

Abstract

Second-order wave effects on the behaviour of ocean platforms have been studied theoretically and experimentally, with particular interest in sum-frequency oscillations of tension leg platforms. These investigations are reviewed in this paper based on the recent works by the author and his co-workers[1)-3)]. The paper consists of two parts.

In Part 1, the complete second-order diffraction theory is formulated for predicting second-order wave loads on arbitrary three-dimensional bodies floating in regular waves. Green's second identity is exploited to express the second-order forces due to the second-order potential in terms of the first-order quantities alone. The resulting expressions for the second-order forces are evaluated from numerical first-order solutions based on the hybrid integral-equation method. Numerical examples are presented for a variety of geometries and compared with previous theoretical and numerical solutions as well as with model test results. Agreement is seen to be satisfactory, illustrating the validity of the proposed approach.

In Part 2, the results are presented of the model tests which were performed in regular waves to measure the second-order sum-frequency oscillations and tether forces of tension leg platforms. These test results are used to validate the predictions based on the complete second-order diffraction theory developed in Part 1. It is found that the vertical-plane motions and resulting tether forces of the tension leg platforms include second-order sum-frequency resonant components which are comparable in magnitude with first-order wave-frequency responses. The correlation between predicted and measured results is overall satisfactory, confirming the validity of the theoretical predictions.

Key words: Nonlinear wave load, second-order diffraction force, wave springing, sum-frequency oscillation, floating body, tension leg platform, vertical-plane motion, tether force

Contents

Part 1. Second-Order Diffraction Theory for Floating Three-Dimensional Bodies 225
1. 1 Introduction 225
1. 2 Statement of boundary-value problem 227
1. 3 Expressions for second-order forces 230
1. 4 Evaluation of double spatial gradients of first-order potentials 232
1. 5 Evaluation of free surface integral 233
1. 5. 1 Integral in near field 233
1. 5. 2 Integral in far field 234
1. 6 Results and discussion 236
1. 6. 1 General numerical procedure 236
1. 6. 2 Comparison with analytical solution for fixed vertical cylinder 238
1. 6. 3 Comparison with results of Kim and Yue for fixed and floating hemisphere 240
1. 6. 4 Comparison with model test results for fixed circular dock and tension leg platform 241
1. 7 Conclusions 244
Part 2. Second-Order Sum-Frequency Oscillations of Tension Leg Platforms 244
2. 1 Introduction 244
2. 2 Theory 245
2. 2. 1 Equations of motion 245
2. 2. 2 Effects of tether system 246
a) Assumptions 246
b) Kinematics of mooring points 247
c) Tether tensions 248
d) Resultant tether forces and moments 248
2. 3 Experiment 250
2. 3. 1 Test set-up 250
2. 3. 2 Generation of waves 252
2. 3. 3 Free oscillation tests in still water 253
2. 3. 4 Tests in regular waves 253
2. 4 Discussion of results 253
2. 4. 1 Natural frequencies and dampings 253
2. 4. 2 Motion responses and tether forces 254
2. 5 Conclusions 262
Acknowledgement 262
References 262
Appendices 264
A Proof of Eq. (1.29) 264
B Damping evaluation from free oscillation decay test 265

Part 1. Second-Order Diffraction Theory for Floating Three-Dimensional Bodies

1. 1 Introduction

The wave loads acting on floating structures in irregular seas include the second-order, high- and low-frequency force components at sum- and difference-frequencies of the wave group, which arise from nonlinearities due to effects of finite wave elevation and finite body motions. These second-order forces may not be large in magnitude compared with first-order excitation at wave frequencies, but can never be ignored due to the possibilities of exciting

resonance frequencies of lightly damped systems. Difference-frequency forces can excite large horizontal excursions of moored structures and large vertical-plane motions of floating structures of small water plane area. Sum-frequency forces can excite resonance oscillations in vertical modes of tension leg platforms.

The prediction of the second-order forces on floating bodies is usually made on the basis of potential flow assumption. The forces can be obtained by integrating the hydrodynamic pressure over the submerged body surface and by retaining terms to second order in wave slope in a consistent perturbation expansion[4]. The resulting expressions for the second-order forces involve the contribution from the second-order velocity potential. To obtain this contribution, one may use two alternative approaches. The first, hereafter designated the direct approach, obtains the forces directly from the integral of the second-order pressure over the submerged body surface[5)-7)]. The second, the indirect approach, uses a reciprocal relation to obtain the second-order forces without the need for explicitly evaluating the second-order potential. Through the use of Green's second identity, the expressions can be obtained for the integrated second-order forces and moments in terms of first-order quantities alone[8),9)]. The direct approach requires the complete solution to the second-order diffraction problem, but once this is evaluated, second-order local quantities such as pressures and surface elevations are readily obtained, in addition to integrated forces and moments. The indirect approach requires only the knowledge of the first-order solution, and is relatively simple in comparison with the direct one. The formulation can be extended to evaluate the second-order pressure distribution[10].

The most difficult and time-consuming part of the solution, common to both approaches, is the efficient and accurate evaluation of the free-surface integral with a highly oscillatory and slowly decaying integrand, which comes from the nonhomogeneity of the second-order free surface condition. Various authors have therefore suggested a methodology for the effective evaluation of this integral. For example, Eatock Taylor and Hung[11] adopted an asymptotical method based on the explicit integration of the leading asymptotic in the far field. Matsui[12),13)], in his calculation of the difference-frequency forces in irregular waves, evaluated exactly the integral over the entire local-wave-free outer domain. He replaced the infinite integral by a finite-interval integral with a rapidly converging series as integrand. To improve the convergence of the series, Euler's transformation was employed. An alternative and more attractive method has been developed recently by Kim and Yue[6),7)], who performed the integration analytically in the infinite local-wave-free domain.

The solution of the second-order diffraction problem has been extensively studied for the case of a fixed vertical cylinder[5),8),9),11),14)]. The method can readily be extended to the second-order forces on axisymmetric bodies[6] and arbitrary three-dimensional bodies[15]. In the extension to the case of floating bodies, additional difficulties arise in the evaluation of the double spatial gradients of the first-order potentials involved in the second-order body surface condition. Molin and Marion[16] obtained some results for floating bodies, but the detail of the calculation method cannot be known. More recently, Kim and Yue[7] formulated a complete second-order diffraction theory, where the second-order sum- and difference-frequency forces were given for fixed and freely floating axisymmetric bodies.

In the following, a more general numerical procedure is developed that allows an efficient and accurate evaluation of the second-order diffraction forces on arbitrary three-dimensional bodies floating in regular waves. The indirect approach is employed to evaluate the forces without the need for the complete solution to the second-order boundary-value problem. The resulting expressions for the second-order forces are evaluated from numerical first-order solutions based on the hybrid integral-equation method. The methodologies are discussed in some detail for the effective evaluation of the free-surface integral and the double

spatial gradients of the first-order potentials involved in the second-order body surface condition. Numerical examples are presented for a variety of geometries and compared with previous theoretical and numerical solutions as well as with model test results.

1. 2 Statement of Boundary-Value Problem

Consider the first- and second-order diffraction of plane regular incident waves by a floating three-dimensional body. The body is allowed to move in response to the first-order wave exciting forces at wave frequency alone. Mean and double-frequency motions caused by the second-order forces are supposed to be completely restrained.

A space-fixed Cartesian coordinate system *oxyz* is defined as shown in Fig. 1.1 with the *oxy*-plane on the mean free surface and the *oz*-axis measured positive vertically upwards. With the assumption of ideal and irrotational flow, the fluid motion is defined by a velocity potential Φ, which can be expressed in the form of the Stokes expansion

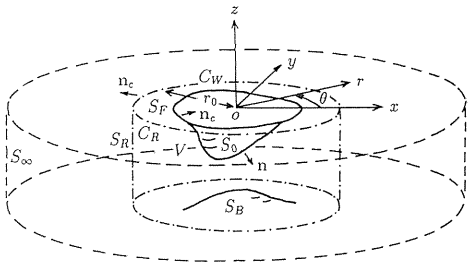

Fig. 1. 1 Coordinate system and fluid boundaries

$$\Phi = \varepsilon\Phi^{(1)} + \varepsilon^2\Phi^{(2)} + O(\varepsilon^3) \tag{1.1}$$

where ε is a perturbation parameter proportional to wave slope. The first-order velocity potential for a regular wave of frequency ω is

$$\Phi^{(1)} = Re[\phi^{(1)}e^{-i\omega t}] \tag{1.2}$$

which can be decomposed into incident and diffraction components

$$\Phi^{(1)} = \Phi_I^{(1)} + \Phi_D^{(1)} = Re[(\phi_I^{(1)} + \phi_D^{(1)})e^{-i\omega t}] \tag{1.3}$$

at time t. For an incident wave of amplitude ζ travelling in the direction $\theta = \alpha$, the first-order complex incident potential is

$$\phi_I^{(1)} = -\frac{ig\zeta}{\omega}\frac{\cosh k(z+h)}{\cosh kh}e^{ik(x\cos\alpha + y\sin\alpha)} \tag{1.4}$$

where g is the acceleration due to gravity, h is the water depth, and k is the wave number that satisfies

$$k \tanh kh = \frac{\omega^2}{g} \equiv \nu \tag{1.5}$$

The problem of the first-order diffraction potential is classical, and a variety of numerical methods of solution is now available.

The first-order body motion vector at a point $\mathbf{x}$ relative to the centre of gravity can be defined by

$$\mathbf{X}^{(1)} = \mathbf{U}^{(1)} + \mathbf{W}^{(1)} \times \mathbf{x} = Re\,[\mathbf{x}^{(1)} e^{-i\omega t}] \tag{1.6}$$

where

$$\mathbf{U}^{(1)} = Re[\mathbf{u}^{(1)} e^{-i\omega t}], \quad \mathbf{W}^{(1)} = Re[\mathbf{w}^{(1)} e^{-i\omega t}] \tag{1.7a,b}$$

are the translation and rotation vectors, respectively, with the components $\mathbf{U}^{(1)} = (\Xi_1, \Xi_2, \Xi_3)$, $\mathbf{W}^{(1)} = (\Xi_4, \Xi_5, \Xi_6)$, and

$$\Xi_j = Re\left[\xi_j e^{-i\omega t}\right], \quad j = 1 \text{ to } 6 \tag{1.7c}$$

The associated second-order velocity potential is defined by

$$\Phi^{(2)} = \Phi_I^{(2)} + \Phi_D^{(2)} \tag{1.8}$$

which fulfills[4]

$$\nabla^2 \Phi^{(2)} = 0 \qquad \text{in the fluid domain } V \tag{1.9a}$$

$$\nabla \Phi^{(2)} \cdot \mathbf{n} = 0 \qquad \text{on the seabed } S_B \tag{1.9b}$$

$$g \frac{\partial \Phi^{(2)}}{\partial z} + \frac{\partial^2 \Phi^{(2)}}{\partial t^2} = -2 \nabla \Phi^{(1)} \cdot \nabla \left(\frac{\partial \Phi^{(1)}}{\partial t} \right) + \frac{\partial}{\partial z} \left(\frac{\partial \Phi^{(1)}}{\partial z} + \frac{1}{g} \frac{\partial^2 \Phi^{(1)}}{\partial t^2} \right) \frac{\partial \Phi^{(1)}}{\partial t} \tag{1.9c}$$

on the free surface S_F

$$\nabla \Phi^{(2)} \cdot \mathbf{n} = -\left[(\mathbf{X}^{(1)} \cdot \nabla) \nabla \Phi^{(1)} \right] \cdot \mathbf{n} + \left(\frac{\partial \mathbf{X}^{(1)}}{\partial t} - \nabla \Phi^{(1)} \right) \cdot (\mathbf{W}^{(1)} \times \mathbf{n}) + \left(\frac{\partial H^{(2)}}{\partial t} \mathbf{x} \right) \cdot \mathbf{n}$$

on the body surface S_0 (1.9d)

where $\mathbf{n}$ is the normal vector directed outwardly from the body, referenced to the body axes.

The matrix $\underline{H}^{(2)}$ is given by

$$\underline{H}^{(2)} = -\frac{1}{2}\begin{bmatrix} \Xi_5^2 + \Xi_6^2 & 0 & 0 \\ -2\Xi_4\Xi_5 & \Xi_4^2 + \Xi_6^2 & 0 \\ -2\Xi_4\Xi_6 & -2\Xi_5\Xi_6 & \Xi_4^2 + \Xi_5^2 \end{bmatrix} \tag{1.10}$$

Eq. (1.10) implies that roll Ξ_4, pitch Ξ_5 and yaw Ξ_6 are taken in that order. The second-order incident potential may be obtained by substituting Eq. (1.4) into the right-hand side of Eq. (1.9c), yielding

$$\Phi_I^{(2)} = Re\,[\phi_I^{(2)} e^{-i2\omega t} + \delta_I^{(2)} t] \tag{1.11}$$

where

$$\phi_I^{(2)} = \frac{i3\omega\zeta^2}{8} \frac{\cosh 2k(z+h)}{\sinh^4 kh} e^{i2k(x\cos\alpha + y\sin\alpha)} \tag{1.12}$$

The constant $\delta_I^{(2)}$ is determined from the requirement that the mean water level be $z = 0$ in an otherwise undisturbed incident wave, giving

$$\delta_I^{(2)} = -\frac{gk\zeta^2}{2\sinh 2kh} \tag{1.13}$$

The analogue expression for the second-order diffraction potential is

$$\Phi_D^{(2)} = Re\left[\phi_D^{(2)} e^{-i2\omega t}\right] \tag{1.14}$$

By substituting Eqs. (1.3), (1.6) ~ (1.8) and (1.11) into Eq. (1.9), the equations governing the second-order diffraction potential $\phi_D^{(2)}$ read

$$\nabla^2\phi_D^{(2)} = 0 \qquad \text{in } V \tag{1.15a}$$

$$\nabla\phi_D^{(2)} \cdot \mathbf{n} = 0 \qquad \text{on } S_B \tag{1.15b}$$

$$\frac{\partial\phi_D^{(2)}}{\partial z} - \frac{4\omega^2}{g}\phi_D^{(2)} = \alpha^{(2)} \qquad \text{on } S_F \tag{1.15c}$$

$$\nabla\phi_D^{(2)} \cdot \mathbf{n} = -\nabla\phi_I^{(2)} \cdot \mathbf{n} + \beta^{(2)} \qquad \text{on } S_0 \tag{1.15d}$$

where

$$\alpha^{(2)} = \frac{i\omega}{g}\left[\nabla\phi^{(1)} \cdot \nabla\phi^{(1)} - \nabla\phi_I^{(1)} \cdot \nabla\phi_I^{(1)} - \frac{1}{2}\phi^{(1)}\left(\frac{\partial^2\phi^{(1)}}{\partial z^2} - k^2\tanh^2 kh\,\phi^{(1)}\right)\right.$$

$$+\frac{1}{2}\phi_I^{(1)}\left(\frac{\partial^2\phi_I^{(1)}}{\partial z^2}-k^2\tanh^2 kh\phi_I^{(1)}\right)\Big] \tag{1.15e}$$

$$\beta^{(2)}=-\frac{1}{2}[(\mathbf{x}^{(1)}\cdot\nabla)\nabla\phi^{(1)}]\cdot\mathbf{n}-\frac{1}{2}(\mathbf{w}^{(1)}\times\mathbf{n})\cdot(i\omega\mathbf{x}^{(1)}+\nabla\phi^{(1)})$$

$$+\frac{i\omega}{2}(\underline{h}^{(2)}\mathbf{x})\cdot\mathbf{n} \tag{1.15f}$$

with

$$\underline{h}^{(2)}=\begin{bmatrix}\xi_5^2+\xi_6^2 & 0 & 0\\ -2\xi_4\xi_5 & \xi_4^2+\xi_6^2 & 0\\ -2\xi_4\xi_6 & -2\xi_5\xi_6 & \xi_4^2+\xi_5^2\end{bmatrix} \tag{1.16}$$

In addition, $\phi_D^{(2)}$ must satisfy the radiation boundary condition ensuring the outgoing wave at infinity. It is shown later that the second-order forces can be evaluated without the need for explicitly solving the boundary-value problem (1.15).

1. 3 Expressions for Second-Order Forces

The wave forces exerted on the body can be obtained by integrating the hydrodynamic pressure over the submerged body surface. By retaining terms up to second order in the integrated pressure, the first- and second-order forces on vertically wall-sided bodies are found to be[4)]

$$\mathbf{F}^{(1)}=\rho\int_{S_0}\frac{\partial\Phi^{(1)}}{\partial t}\mathbf{n}dS \tag{1.17}$$

$$\mathbf{F}^{(2)}=\rho\int_{S_0}\left[\frac{\partial\Phi^{(2)}}{\partial t}+\frac{1}{2}|\nabla\Phi^{(1)}|^2+\mathbf{X}^{(1)}\cdot\nabla\left(\frac{\partial\Phi^{(1)}}{\partial t}\right)\right]\mathbf{n}dS$$

$$-\frac{\rho g}{2}\oint_{CW}\zeta_R^{(1)2}\mathbf{n}dl+\mathbf{W}^{(1)}\times\left(m\frac{d^2\mathbf{U}^{(1)}}{dt^2}\right)-\frac{\rho g}{2}A_W(x_f\Xi_4+y_f\Xi_5)\Xi_6\mathbf{e}_3 \tag{1.18}$$

where $\zeta_R^{(1)}$ is the first-order relative wave elevation defined by

$$\zeta_R^{(1)}=-\frac{1}{g}\frac{\partial\Phi^{(1)}}{\partial t}-\mathbf{X}^{(1)}\cdot\mathbf{e}_3=Re[\eta_R^{(1)}e^{-i\omega t}] \tag{1.19}$$

along the mean waterline C_W, ρ is the fluid density, m is the mass of body, A_W is the water plane area, (x_f, y_f) are the coordinates of the centre of flotation, and e_j $(j=1,2,3)$ are the unit vectors in the direction of the space-fixed coordinate axes.

The terms in Eq. (1.18), depending on quadratic products of the first-order effects, can be decomposed into a mean ($\mathbf{F}_m^{(2)}$) and time oscillatory component ($\mathbf{F}_o^{(2)}$) respectively, such that

$$\mathbf{F}_m^{(2)} = Re\left[\frac{\rho}{2}\iint_{S_0}\left(\frac{1}{2}\nabla\phi^{(1)} \cdot \nabla\phi^{(1)*} - i\omega\nabla\phi^{(1)} \cdot \mathbf{x}^{(1)*}\right)\mathbf{n}\,dS - \frac{\rho g}{4}\oint_{C_W}\eta_R^{(1)}\eta_R^{(1)*}\mathbf{n}\,dl - \frac{m\omega^2}{2}\mathbf{w}^{(1)}\times\mathbf{u}^{(1)*} - \frac{\rho g}{4}A_W(x_f\xi_4 + y_f\xi_5)\xi_6^*\mathbf{e}_3\right] \tag{1.20}$$

$$\mathbf{F}_o^{(2)} = Re\left\{\left[\frac{\rho}{2}\iint_{S_0}\left(\frac{1}{2}\nabla\phi^{(1)} \cdot \nabla\phi^{(1)} - i\omega\nabla\phi^{(1)} \cdot \mathbf{x}^{(1)}\right)\mathbf{n}\mathrm{dS} - \frac{\rho g}{4}\oint_{C_W}\eta_R^{(1)2}\mathbf{n}\,dl - \frac{m\omega^2}{2}\mathbf{w}^{(1)}\times\mathbf{u}^{(1)} - \frac{\rho g}{4}A_W(x_f\xi_4 + y_f\xi_5)\xi_6\mathbf{e}_3\right]e^{-i2\omega t}\right\} \tag{1.21}$$

where * denotes the complex conjugate. The calculation of $\mathbf{F}_m^{(2)}$ and $\mathbf{F}_o^{(2)}$ is straightforward for any body for which the first-order solution is known.

The remaining term in Eq. (1.18), namely

$$\mathbf{F}_q^{(2)} = \rho\iint_{S_0}\frac{\partial\Phi^{(2)}}{\partial t}\mathbf{n}\,dS \tag{1.22}$$

can be evaluated in the manner suggested by Lighthill[8] and Molin[9]. To do this, use is made of the auxiliary first-order radiation potential ψ_j, associated with a unit oscillation of the body in the direction $\mathbf{e}_j$ at double frequency 2ω. By applying Green's second identity, and making use of Eqs. (1.15a ~ d) and radiation boundary condition for $\phi_D^{(2)}$, $\mathbf{F}_q^{(2)}$ can be expressed in terms of the first-order quantities alone, such that

$$\mathbf{F}_q^{(2)} = Re\left[(\mathbf{F}_{qI} + \mathbf{F}_{qII} + \mathbf{F}_{qIII} + \mathbf{F}_{qIV})e^{-i2\omega t}\right] + \rho A_W\delta_I^{(2)}\mathbf{e}_3 \tag{1.23}$$

where

$$\mathbf{F}_{qI} = -2i\rho\omega\iint_{S_0}\phi_I^{(2)}\mathbf{n}\,dS \tag{1.24}$$

$$\mathbf{F}_{qII} = \sum_{j=1}^{3}\left(2i\rho\omega\iint_{S_0}\psi_j\nabla\phi_I^{(2)} \cdot \mathbf{n}\,dS\right)\mathbf{e}_j \tag{1.25}$$

$$\mathbf{F}_{qIII} = \sum_{j=1}^{3}\left(-2i\rho\omega\iint_{S_0}\psi_j\beta^{(2)}dS\right)\mathbf{e}_j \tag{1.26}$$

$$\mathbf{F}_{qIV} = \sum_{j=1}^{3}\left(2i\rho\omega\iint_{S_F}\psi_j\alpha^{(2)}dS\right)\mathbf{e}_j \tag{1.27}$$

The calculation of $\mathbf{F}_{qI}$ and $\mathbf{F}_{qII}$ is straightforward as $\phi_I^{(2)}$ is known and ψ_j can be obtained from the first-order solution. The difficulty, however, arises in the evaluation of $\mathbf{F}_{qIII}$ involving the double spatial gradients of the first-order potentials, for which accurate solutions are difficult

to obtain by existing numerical methods. Moreover, in order to evaluate $\mathbf{F}_{qIV}$, the integration must be performed over an infinite area of the free surface, but this is not trivial because the integrand displays a highly oscillatory and slowly decaying behaviour.

1. 4 Evaluation of Double Spatial Gradients of First-Order Potentials

The double spatial gradients of the first-order potentials involved in $\mathbf{F}_{qIII}$ can be reduced to single gradients by virture of Stokes' theorem

$$\iint_{S_0} \nabla \times (\psi_j \mathbf{x}^{(1)} \times \nabla \phi^{(1)}) \cdot \mathbf{n} dS = \oint_{C_W} (\psi_j \mathbf{x}^{(1)} \times \nabla \phi^{(1)}) \cdot d\mathbf{l} \tag{1.28}$$

where the vector $d\mathbf{l}$ is directed as indicated in Fig. 1.2. Using the well-known formulas of vector analysis, and by virtue of the assumption of irrotational and ideal flow, it follows that[19)]

$$\begin{aligned} &\iint_{S_0} \psi_j \left[(\mathbf{x}^{(1)} \cdot \nabla) \nabla \phi^{(1)} \right] \cdot \mathbf{n} dS \\ &= \iint_{S_0} \left[(x^{(1)} \cdot \mathbf{n})(\nabla \psi_j \cdot \nabla \phi^{(1)}) - (\mathbf{x}^{(1)} \cdot \nabla \psi_j)(\mathbf{n} \cdot \nabla \phi^{(1)}) \right. \\ &\left. - \psi_j (\mathbf{w}^{(1)} \times \mathbf{n}) \cdot \nabla \phi^{(1)} \right] dS - \oint_{C_W} (\psi_j \mathbf{x}^{(1)} \times \nabla \phi^{(1)}) \cdot d\mathbf{l} \end{aligned} \tag{1.29}$$

which allows the double spatial gradients of the potential $\phi^{(1)}$ to be replaced by single gradients of $\phi^{(1)}$ and the auxiliary potential ψ_j. The details of derivation of Eq. (1.29) are given in Appendix A.

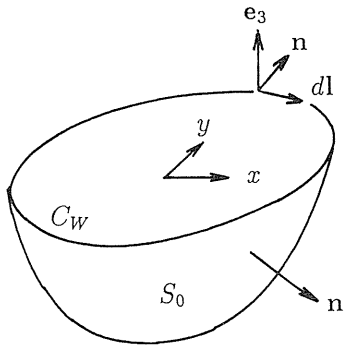

Fig. 1. 2 Definition of geometry for Stokes' theorem

For wall-sided bodies that intersect the free surface at right angles, the vector $d\mathbf{l}$ is horizontal and defined by

$$d\mathbf{l} = (\mathbf{n} \times \mathbf{e}_3) dl \tag{1.30}$$

The line integral on the right-hand side of Eq. (1.29) can then be given by

$$\oint_{C_W} (\psi_j \mathbf{x}^{(1)} \times \nabla\phi^{(1)}) \cdot d\mathbf{l} = \oint_{C_W} \psi_j \left[(\mathbf{x}^{(1)} \cdot \mathbf{n}) \frac{\partial\phi^{(1)}}{\partial z} - (\mathbf{x}^{(1)} \cdot \mathbf{e}_3) \frac{\partial\phi^{(1)}}{\partial n} \right] dl \quad (1.31)$$

Combining Eqs. (1.15f), (1.29) and (1.31) with Eq. (1.26), $\mathbf{F}_{qIII}$ can be rewritten in the form

$$\begin{aligned} \mathbf{F}_{qIII} = \sum_{j=1}^{3} \Big\{ & i\rho\omega \iint_{S_0} \Big[(\mathbf{x}^{(1)} \cdot \mathbf{n})(\nabla\psi_j \cdot \nabla\phi^{(1)}) - (\mathbf{x}^{(1)} \cdot \nabla\psi_j)(\mathbf{n} \cdot \nabla\phi^{(1)}) \\ & + i\omega\psi_j (\mathbf{w}^{(1)} \times \mathbf{n}) \cdot \mathbf{x}^{(1)} + \frac{i\omega}{2} (\underline{h}^{(2)} \mathbf{x}) \cdot \mathbf{n} \Big] dS \\ & - i\rho\omega \oint_{C_W} \psi_j \left[(\mathbf{x}^{(1)} \cdot \mathbf{n}) \frac{\partial\phi^{(1)}}{\partial z} - (\mathbf{x}^{(1)} \cdot \mathbf{e}_3) \frac{\partial\phi^{(1)}}{\partial n} \right] dl \Big\} \end{aligned} \quad (1.32)$$

which is more desirable for numerical evaluation.

1. 5 Evaluation of Free-Surface Integral

For the evaluation of the free-surface integral of Eq. (1.27), it is convenient to separate the free surface S_F into the discretised domain S_{F1} close to the body and the infinite outer domain S_{F2}. The integral over the discretised domain can then be evaluated by numerical quadrature, while it is handled asymptotically for the infinite domain as described later.

1. 5. 1 Integral in near field

The free-surface integral consists of a summation of integrals of the general form

$$\iint_{S_F} \psi_j D_1\phi_1^{(1)} D_2\phi_2^{(1)} dS \quad (1.33)$$

where D_1 and D_2 are differential operators defined by Eq. (1.15e). Either one or both of the potentials $\phi_1^{(1)}$ and $\phi_2^{(1)}$ are diffraction potentials. These integrals in the discretised domain can be evaluated accurately by numerical quadrature (e.g., a four-point Gaussian quadrature) if the integrand involves only the single spatial gradients of the potentials.

In order to evaluate the integrals involving the double spatial gradients, it is useful to reduce the double derivatives to single derivatives by virtue of Green's theorem in two-dimensions. This yields

$$\begin{aligned} \iint_{S_{F1}} \psi_j \phi_1^{(1)} \frac{\partial^2\phi_2^{(1)}}{\partial z^2} dS &= -\iint_{S_{F1}} \psi_j \phi_1^{(1)} \left(\frac{\partial^2\phi_2^{(1)}}{\partial x^2} + \frac{\partial^2\phi_2^{(1)}}{\partial y^2} \right) dS \\ &= \iint_{S_{F1}} \left[\frac{\partial(\psi_j\phi_1^{(1)})}{\partial x} \frac{\partial\phi_2^{(1)}}{\partial x} + \frac{\partial(\psi_j\phi_1^{(1)})}{\partial y} \frac{\partial\phi_2^{(1)}}{\partial y} \right] dS \\ &\quad - \oint_{C_W + C_R} \psi_j \phi_1^{(1)} \frac{\partial\phi_2^{(1)}}{\partial n_c} dl \end{aligned} \quad (1.34)$$

where C_R is a fictitious circular boundary separating the free surface into the two domains,

and n_c denotes the normal directed outwardly from C_W and C_R (refer to Fig. 1.1). As the integrand of Eq. (1.34) involves only single derivatives of $\phi^{(1)}$ and ψ_j, the integral may be evaluated accurately from solutions based on conventional numerical first-order analysis.

1. 5. 2 Integral in far field

The integrals (1.33) over the infinite outer domain may be evaluated by means of an asymptotic method as employed by Matsui[12),13)] to calculate the difference-frequency forces in bichromatic waves. This is briefly redescribed for the special case

$$I = \iint_{S_{F2}} \psi_j \phi_D^{(1)2} dS \tag{1.35}$$

For the sake of compactness, the wave flow is assumed to be symmetric with respect to $\theta = 0$. Away from the body the potentials may be written as

$$\phi_D^{(1)} = \sum_{n=0}^{\infty} \varepsilon_n \left[A_n(z) \mathrm{H}_n^{(1)}(kr) + \sum_{m=1}^{\infty} A_{nm}(z) \mathrm{K}_n(k_m r) \right] \cos n\theta = \phi_D^H + \phi_D^K \tag{1.36}$$

$$\psi_j = \sum_{n=0}^{\infty} \varepsilon_n \left[\alpha_n(z) \mathrm{H}_n^{(1)}(\kappa r) + \sum_{m=1}^{\infty} \alpha_{nm}(z) \mathrm{K}_n(\kappa_m r) \right] \cos n\theta = \psi^H + \psi^K \tag{1.37}$$

where $\varepsilon_n = 1$ for $n = 0$, otherwise $\varepsilon_n = 2$, $\mathrm{H}_n^{(1)}$ is the Hankel function of the first kind of order n, K_n is the modified Bessel function of the second kind of order n, and k_m, κ and κ_m denote the real positive roots of the equations

$$k_m \tan k_m h = -\frac{\omega^2}{g} \tag{1.38}$$

$$\kappa \tanh \kappa h = \frac{4\omega^2}{g} \tag{1.39}$$

$$\kappa_m \tan \kappa_m h = -\frac{4\omega^2}{g} \tag{1.40}$$

The second terms of Eqs. (1.36) and (1.37), ϕ_D^K, ψ^K, represent local (evanescent) modes that decay exponentially with the radial distance, and the far-field asymptotics of the potentials are given only by the first terms, ϕ_D^H, ψ^H, which represent propagating waves.

The integral (1.35) may now be evaluated over two intervals, (r_0, r_1) and (r_1, ∞), where r_0 is the radius of the fictitious boundary C_R, and the radius r_1 is chosen so that the influence of local modes vanishes in the latter interval

$$I = \int_0^{2\pi} d\theta \left\{ \int_{r_0}^{r_1} \psi_j \phi_D^{(1)2} r dr + \int_{r_1}^{\infty} \psi^H (\phi_D^H)^2 r dr + \int_{r_1}^{\infty} \left[\psi_j \phi_D^{(1)2} - \psi^H (\phi_D^H)^2 \right] r dr \right\} \tag{1.41}$$

The first integral in Eq. (1.41) over the finite interval (r_0,r_1) can be computed numerically. The last integral is made negligibly small by a suitable choice of the partition radius r_1.

The second integral over the infinite domain

$$I_2 = \int_0^{2\pi} d\theta \int_{r_1}^{\infty} \psi^H (\phi_D^H)^2 r dr \tag{1.42}$$

may be evaluated in the following manner. The integral is first executed over the azimuthal angle θ. By substituting Eqs. (1.36) and (1.37) into Eq. (1.42) and integrating over θ using the method of stationary phase, one obtains

$$I_2 = \pi \sum_{n=0}^{\infty} \sum_{m=0}^{\infty} \varepsilon_n \varepsilon_m A_n(0) \left[\alpha_{|n-m|}(0) I(n,m,|n-m|) + \alpha_{n+m}(0) I(n,m,n+m)\right] \tag{1.43}$$

where

$$I(n,m,l) = \int_{r_1}^{\infty} \mathrm{H}_n^{(1)}(kr)\mathrm{H}_m^{(1)}(kr)\mathrm{H}_l^{(1)}(\kappa r) r dr \tag{1.44}$$

At large radius one may use the large argument asymptotic form of Hankel function[17)]

$$\mathrm{H}_n^{(1)}(x) \sim \left(\frac{2}{\pi x}\right)^{\frac{1}{2}} h_n(x) \mathrm{e}^{i(x-\chi_n)} \tag{1.45}$$

where

$$h_n(x) = 1 + \sum_{s=1}^{\infty} i^s \frac{(4n^2-1^2)(4n^2-3^2)\cdots[4n^2-(2s-1)^2]}{s!(8x)^{2s}} \tag{1.46}$$

and $\chi_n = (2n+1)\pi/4$. When this is substituted into Eq. (1.44), one obtains

$$I(n,m,l) = \int_{r_1}^{\infty} F(r) \mathrm{e}^{iqr} dr \tag{1.47}$$

where

$$F(r) = \frac{2}{\pi k}\left(\frac{2}{\pi \kappa r}\right)^{\frac{1}{2}} \mathrm{e}^{-i\chi_{n+m+l}} h_n(kr) h_m(kr) h_l(\kappa r) \tag{1.48}$$

$$q = 2k + \kappa \tag{1.49}$$

By virtue of the periodic nature of the exponential function of pure complex argument, the infinite integral (1.47) can be replaced by a finite-interval integral

$$I(n,m,l) = \int_{r_1}^{r_1 + \frac{\pi}{q}} G(r) e^{iqr} dr \tag{1.50}$$

where

$$G(r) = \sum_{s=0}^{\infty} (-1)^s F\left(r + \frac{s\pi}{q}\right) \tag{1.51}$$

Since $F(r)$ decreases as $r^{-1/2}$, it is difficult to obtain a converged solution by direct summation of the series (1.51). The convergence may, however, be improved if the series is replaced by Euler's transformation[17]

$$\sum_{s=0}^{\infty} (-1)^s F_s = \sum_{s=0}^{\infty} (-1)^s \frac{\triangle^s F_0}{2^{s+1}} \tag{1.52}$$

where

$$F_s = F\left(r + \frac{s\pi}{q}\right) \tag{1.53}$$

and $\triangle^s F_0$ is the s-th difference of F_0 given by

$$\triangle^s F_0 = \sum_{t=0}^{\infty} (-1)^t \binom{s}{t} F_{s-t} \tag{1.54}$$

One may note that the convergence rate of the series (1.52) is more rapid for F_s that decays more slowly with increasing s. The convergence can further be improved if Euler's transformation is applied after the first few (say M) terms of the series (1.51) are directly summed

$$\sum_{s=0}^{\infty} (-1)^s F_s = \sum_{s=0}^{M-1} (-1)^s F_s + \sum_{s=0}^{\infty} (-1)^{s+M} \frac{\triangle^s F_M}{2^{s+1}} \tag{1.55}$$

The finite integral of Eq. (1.50) can then be evaluated to any desirable degree of accuracy by applying numerical quadrature (e.g., a Newton-Cotes 9-point rule).

1. 6 Results and Discussion

1. 6. 1 General numerical procedure

The theory described in the foregoing was applied to develop a general numerical procedure for computing the second-order wave exciting forces on arbitrary three-dimensional bodies floating in regular waves. The expressions derived for the second-order forces were evaluated from numerical first-order solutions based on the hybrid integral-equation method, described by Matsui and Kato[18]. Fig. 1.3 illustrates typical idealisations for the hybrid integral-equation method. The fluid region was divided into two regions by introducing a fictitious vertical cylinder enclosing the body. The boundary surfaces inside the fictitious cylinder were discretised into quadratic isoparametric elements with 8 nodes, while an analytical

solution based on the eigenfunction expansion in cylindrical coordinates was employed for the infinite outside region. Based on the results of systematic convergence tests (Tables 1.1 and 1.2), the double series of eigenfunction expansion were truncated at 9th Fourier harmonics in θ and at 14 evanescent modes in z. The double symmetry of the body geometry was exploited.

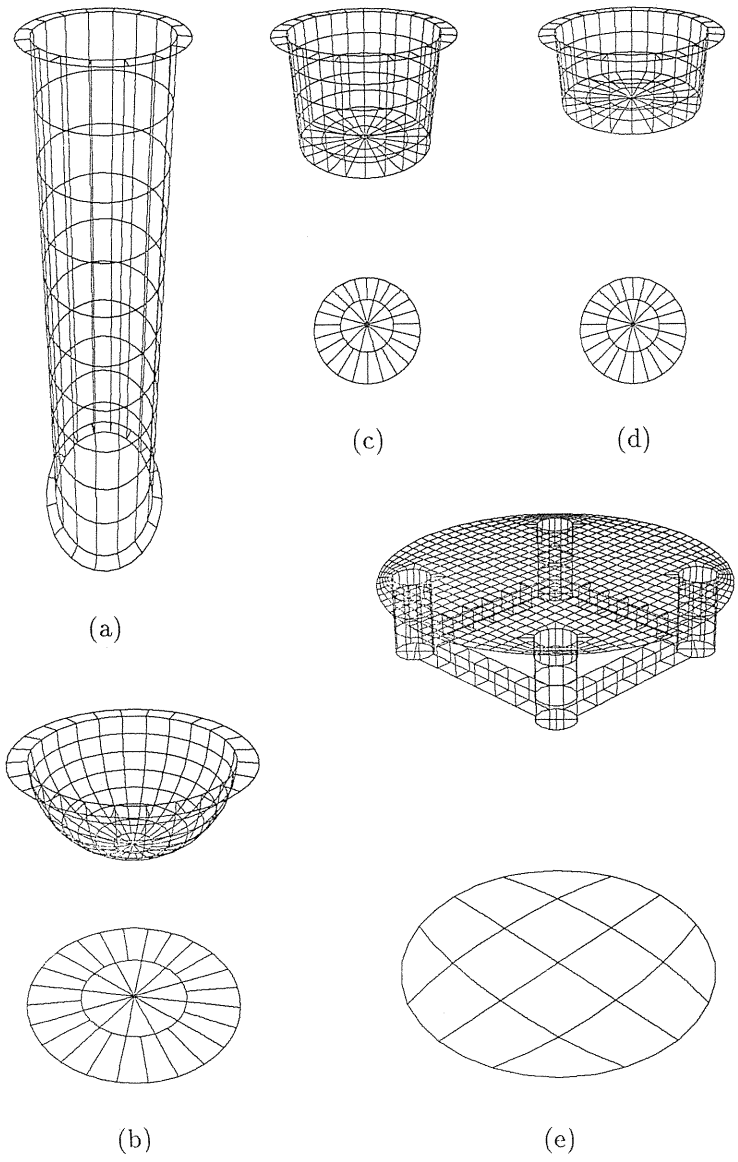

Fig. 1.3 Boundary element idealisations for (a) vertical cylinder, (b) floating hemisphere, (c) circular dock (draft=25 cm), (d) circular dock (draft=15 cm), (e) tension leg platform

Table 1.1 Second-order horizontal force $F_x^{(2)}$ and moment $M_y^{(2)}$ on fixed vertical cylinder computed with increasing N and M (where N and M denote maximum terms of Fourier-series and evanescent modes in double series of eigenfunction expansion)

N	M	$\lvert F_x^{(2)}\rvert/(\rho g a \zeta^2)$		$\lvert M_y^{(2)}\rvert/(\rho g a^2 \zeta^2)$	
		$ka = 1.0$	$ka = 2.5$	$ka = 1.0$	$ka = 2.5$
5	10	1.6050	4.5931	3.5870	15.035
7	10	1.6050	4.5955	3.5870	15.043
9	10	1.6050	4.5955	3.5870	15.043
5	12	1.6097	4.5917	3.5942	15.006
7	12	1.6097	4.5941	3.5942	15.014
9	12	1.6097	4.5941	3.5942	15.014
5	14	1.6088	4.5892	3.5951	14.998
7	14	1.6088	4.5915	3.5951	15.006
9	14	1.6088	4.5915	3.5951	15.006
Analytical		1.6454	4.6444	3.6263	15.069

Table 1.2 Second-order horizontal force and moment on fixed vertical cylinder computed with increasing mesh subdivisions (where N_s denotes number of elements on cylinder surface)

N_S	$\lvert F_x^{(2)}\rvert/(\rho g a \zeta^2)$		$\lvert M_y^{(2)}\rvert/(\rho g a^2 \zeta^2)$	
	$ka = 1.0$	$ka = 2.5$	$ka = 1.0$	$ka = 2.5$
72	1.5920	4.5151	3.5623	14.675
128	1.6084	4.5877	3.5931	14.979
200	1.6088	4.5915	3.5951	15.006
Analytical	1.6454	4.6444	3.6263	15.069

1. 6. 2 Comparison with analytical solutions for fixed vertical cylinder

Although the present numerical procedure has been developed without any restriction on the body shape, the geometry studied first is a uniform vertical circular cylinder fixed at the seabed and having a depth-to-radius radio of $h/a = 10.0$. This case was selected to check the validity of the numerical procedure by comparison with the analytical solution for the second-order double-frequency force[11]. Some results of couvergence tests are presented in Tables 1.1 and 1.2, where the double-frequency horizontal force and moment on the cylinder were computed with increasing mesh subdivisions and numbers of terms in the eigenfunction series. These results are found to ensure good convergence of the present numerical solutions. Fig. 1.4 shows the computed results for the transfer function of double-frequency horizontal force, which are compared with the corresponding analytical solutions. Agreement

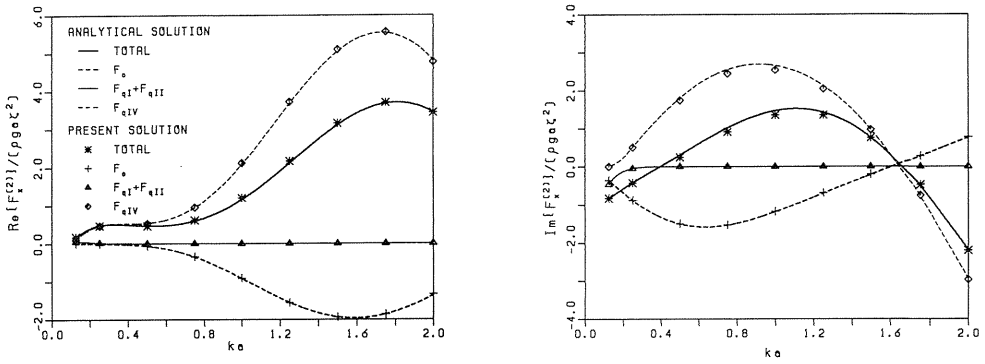

Fig. 1.4 Comparison between analytical and numerical results for second-order horizontal force on fixed vertical cylinder; (a) in-phase component, (b) out-of-phase component

Table 1.3 Contribution of free-surface integral to second-order horizontal force on fixed vertical cylinder (r_0/a=1.2, ka=1.0)

r_1/a	Local wave effects included	Local wave effects excluded
3	3.425+2.406i	4.236+1.564i
4	3.228+2.538i	4.236+1.564i
5	3.128+2.546i	4.236+1.564i
6	3.069+2.570i	4.236+1.564i
8	2.997+2.596i	4.236+1.564i
10	2.960+2.607i	4.236+1.564i
12	2.938+2.614i	4.236+1.564i
16	2.916+2.620i	4.236+1.564i
20	2.907+2.623i	4.236+1.564i

between analytical and numerical predictions is seen to be excellent over the frequency range examined, confirming the validity and accuracy of the present numerical procedure.

In order to show the effectiveness of the proposed method for evaluating the free-surface integral, Table 1.3 gives the results for the contribution of the free-surface integral to the second-order horizontal force on the cylinder. Both the results including and excluding the local wave effects are presented with increasing the partition radius r_1. It can be noted that the integral excluding the local wave effects takes a stationary value, irrespective of r_1, demonstrating the effectiveness and high accuracy of the method discussed in the preceding section for evaluating the integral in the infinite local-wave-free domain. As the local wave effects decay exponentially with the radial distance, the integral including these effects is found to approach quickly to the asymptotic value with increasing r_1.

1. 6. 3 Comparison with results of Kim and Yue for fixed and floating hemisphere

The geometry studied next is a hemisphere fixed and floating near the free surface and having a depth-to-radius ratio of $h/a = 3.0$. Figs. 1.5 ~ 1.8 show the computed results for the double-frequency horizontal and vertical forces on the sphere. This case has also been investigated numerically by Kim and Yue[7], whose results are also plotted in the figures for comparison. Agreement is observed to be satisfactory, illustrating again the validity of the present numerical procedure.

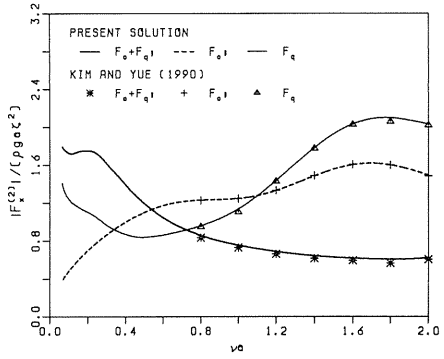

Fig. 1.5 Comparison with results of Kim and Yue for second-order horizontal force on fixed hemisphere

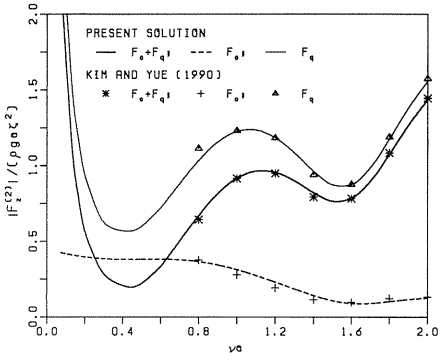

Fig. 1.6 Comparison with results of Kim and Yue for second-order vertical force on fixed hemisphere

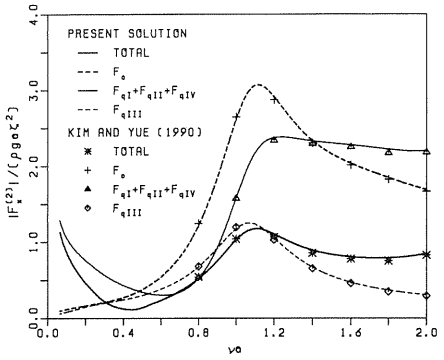

Fig. 1.7 Comparison with results of Kim and Yue for second-order horizontal force on floating hemisphere

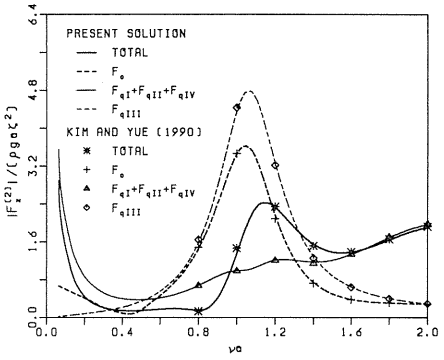

Fig. 1.8 Comparison with results of Kim and Yue for second-order vertical force on floating hemisphere

1. 6. 4 Comparison with model test results for fixed circular dock and tension leg platform

To give experimental evidence on the validity of the present numerical procedure, the model tests were conducted to measure the second-order wave forces on a fixed circular dock and a tension leg platform (TLP). The principal dimensions of the experimental models are presented in Table 1.4 and in Fig. 1.9. The tests were made in the wave tank at Nagoya University. This facility has a width of 2 m, a nominal water depth of 1 m, and a distance of approximately 15 m between wavemaker and beach. The models were fixed near the free surface at the distance of approximately 6 m from the beach, through a load cell with a nominal capacity of 5 kgf for force and 2 kgfm for moment. The tests were carried out in regular waves for ranges of wave frequencies (0.54 ~ 1.56 Hz) and amplitudes (1.5 ~ 5 cm). The second-order force components at double frequency were filtered out from the measured time histories of forces by a harmonic analysis based on the Fast Fourier Transform algorithm.

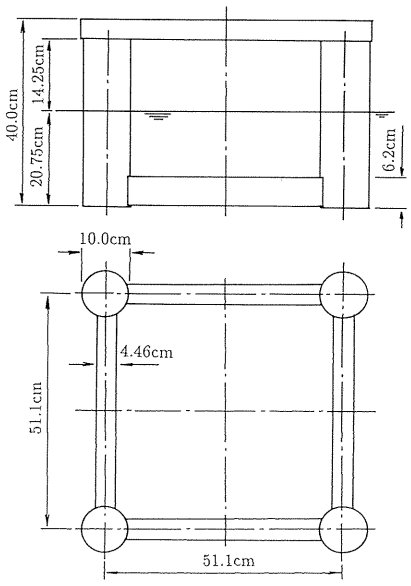

Fig. 1.9 Layout of tension leg platform model

Figs. 1.10 ~ 1.21 show the comparison of computed and measured second-order horizontal and vertical forces, and moment about the horizontal axis passing through the centre of flotation ($x = y = z = 0$). Both the results computed with and without the second-order potential effects are presented and compared. It is observed that the contribution of the second-order potential is significant over the entire frequency range. An approximate second-order theory neglecting these effects is found to substantially underestimate the heave and pitch excitation forces. The correlation between theory and experiment is considered to be generally satisfactory, in view of the small magnitudes of the forces being measured. Significant discrepancies observed in the high-frequency range are thought to be caused by the reflections of standing waves from the side walls of the tank[20].

Table 1.4 Principal dimensions of experimental models

Description (Symbol)	Value		Unit
	Circular dock	TLP	
Column diameter (2a)	30	10	cm
Draft (d)	15 and 25	20.75	cm
Spacing between column centre lines (L)	–	51.1	cm
Water depth (h)	100	120	cm
Wave direction (α)	0°	0° and 45°	

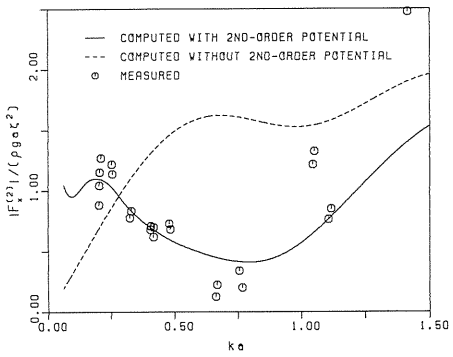

Fig. 1.10 Comparison between computed and measured results for second order horizontal force on fixed circular dock (draft=25 cm)

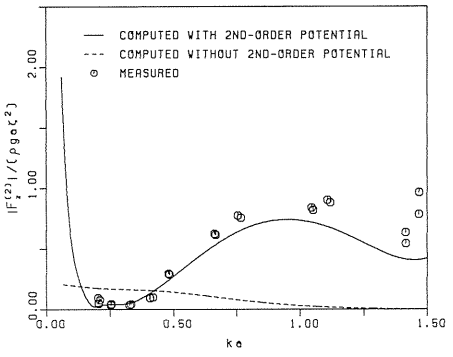

Fig. 1.11 Comparison between computed and measured results for second-order vertical force on fixed circular dock (draft=25 cm)

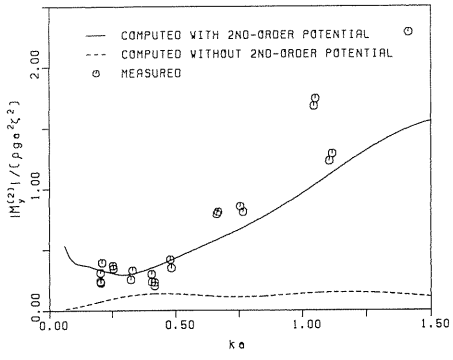

Fig. 1.12 Comparison between computed and measured results for second-order moment about horizontal axis on fixed circular dock (draft=25 cm)

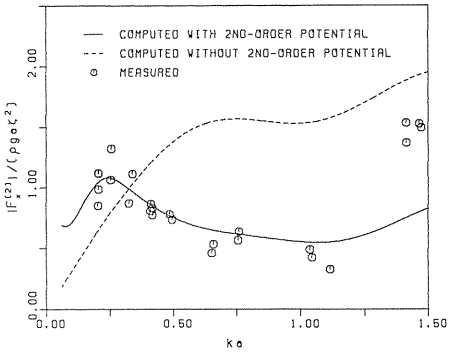

Fig. 1.13 Comparison between computed and measured results for second-order horizontal force on fixed circular dock (draft=15 cm)

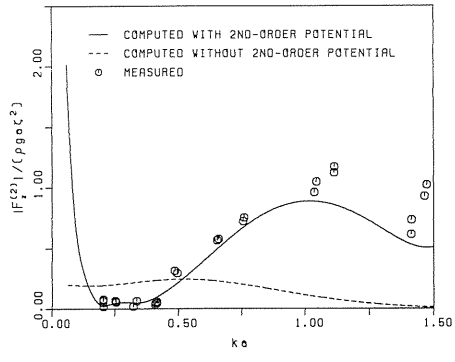

Fig. 1.14 Comparison between computed and measured results for second-order vertical force on fixed circular dock (draft=15 cm)

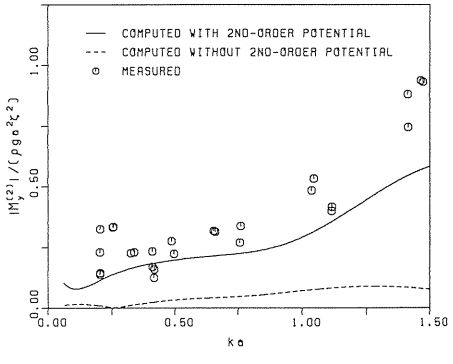

Fig. 1.15 Comparison between computed and measured results for second-order moment about horizontal axis on fixed circular dock (draft=15 cm)

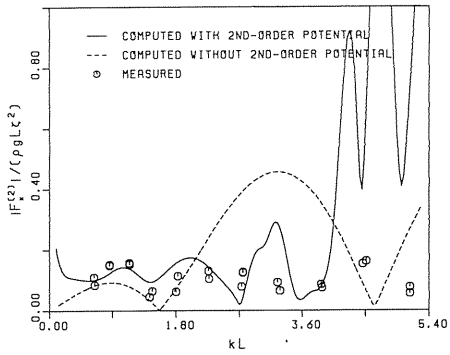

Fig. 1.16 Comparison between computed and measured results for second-order surge force on fixed TLP in head waves

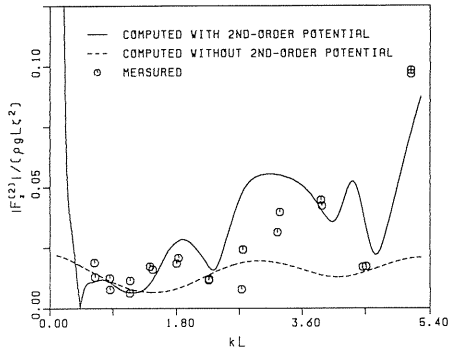

Fig. 1.17 Comparison between computed and measured results for second-order heave force on fixed TLP in head waves

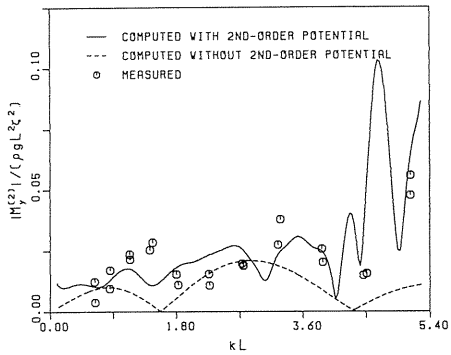

Fig. 1.18 Comparison between computed and measured results for second-order pitch moment on fixed TLP in head waves

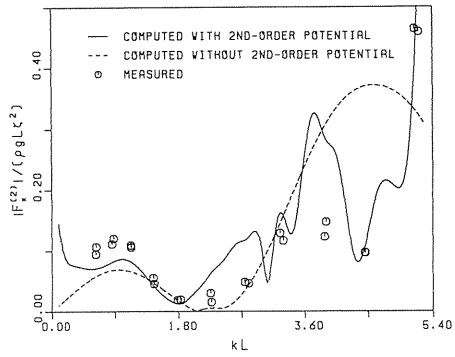

Fig. 1.19 Comparison between computed and measured results for second-order surge force on fixed TLP in bow-quartering waves

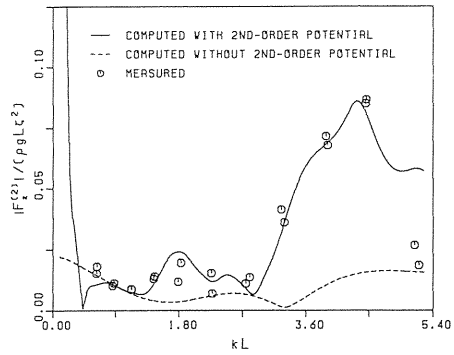

Fig. 1.20 Comparison between computed and measured results for second-order heave force on fixed TLP in bow-quartering waves

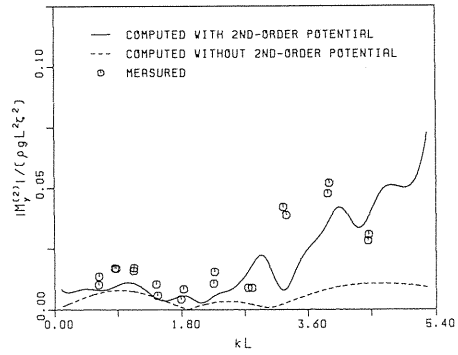

Fig. 1.21 Comparison between computed and measured results for second-order pitch moment on fixed TLP in bow-quartering waves

1. 7 Conclusions

An efficient and accurate numerical procedure was developed to compute the second-order diffraction forces on floating bodies of arbitrary form in regular waves. Green's second identity was exploited to obtain the forces without the need for explicitly evaluating the second-order potential. The resulting expressions for the second-order forces were evaluated from numerical first-order solutions based on the hybrid integral-equation method. The methodologies were discussed in some detail for the effective evaluation of the free-surface integral with an oscillatory and slowly decaying integrand, and the double spatial gradients of the first-order potentials involved in the second-order body surface condition. The validity of the numerical procedure was confirmed by comparison of computed results with previous analytical and numerical solutions as well as with model test results for the fixed circular dock and tension leg platform. The present numerical procedure may readily be extended to calculate the sum- and difference-frequency forces in irregular waves[13].

An important finding in the present numerical studies is that the second-order sum-frequency forces are dominated by the contribution of the second-order potential. An approximate second-order theory using second-order contributions due to the first-order potentials only was found to substantially underestimate the second-order heave and pitch excitation forces, which may cause the vertical-plane resonant oscillations of tension leg platforms.

Part 2. Second-Order Sum-Frequency Oscillations of Tension Leg Platforms

2. 1 Introduction

The deep water tension leg platform (TLP) is designed such that the natural periods of the vertical-plane motions (typically 1 ~ 3 seconds) are substantially below the wave periods. Also, the damping of the system is low. Besides the wave frequency responses, the resonant vertical-plane oscillations and resulting tensions in the tethers, caused by any source of high frequency excitations, then become critical for the design of the TLP. It is now widely recognized that the second-order sum-frequency wave exciting forces, often called 'springing' forces, are a primary source of such high-frequency resonant excitations. Thus, besides the need for better estimates of the damping forces, a reliable prediction of these nonlinear wave excitations is critical for the design of the TLP tethers against fatigue damage.

During the last fifteen years, considerable progress has been made on the development of the second-order wave diffraction theory and computations[4),6),7)]. Despite such progresses, it is only recently that the complete calculations of the second-order sum-frequency wave excitations on a full TLP have been reported[1),3),21)]. A primary reason is theoretical and computational difficulties in obtaining the solution of second-order sum-frequency potential. Thus, the previous calculations of springing forces on the TLP have been based on some simplifying approximations. For example, Yoshida *et al.*[22)] have taken into account only the second-order contribution due to change of the wetted body surface along the waterline. Petrauskas and Liu[23)] have completely neglected the effects of second-order potential. De Boom, Pinkster and Tan[24)] have included the second-order incident potential contribution but neglected that of the diffraction counterparts. Consequently, large discreancies were observed between predicted and measured results for the high-frequency wave excitations and responses of the TLP. For example, measured rms values of the tether forces reported by Petrauskas and Liu[23)] were three or more times larger than predictions using experimental damping values.

The complete calculation of the nonlinear sum-frequency wave excitations on a TLP was first attempted by Kim and Yue[25)]. Based on their complete second-order diffraction theory

for axisymmetric bodies[6], they obtained the sum-frequency wave loads on a single TLP column and applied those results to the dynamic analysis of a full TLP through a simple approximation method (e.g., multiplying the single-leg results by the number of columns to estimate the wave loads on the full TLP). The computed rms values of the tether force were found to be two to three times higher than that predicted by an approximate second-order theory using second-order contributions due to first-order potentials only. However, the wave interaction between columns and the pontoon effects are ignored in their estimation.

The full three-dimensional analyses of the second-order sum-frequency wave loads on a fixed TLP have been reported more recently by Kim[21] and Matsui, Suzuki and Sakoh[1]. Through comparison of the full TLP results with approximate evaluations based on the results of a single column (Kim and Yue[25]) and four columns only (Chau[26]), Kim[21] has shown that both the wave interaction between columns and the effect of pontoons are important to the calculation of the springing forces on the TLP. Matsui *et al.*[1] have attempted also comparison of their numerical results with the model test results obtained by themselves. Satisfactory agreement was observed between computed and measured results, promising the usefulness of the complete second-order diffraction theory for predicting the sum-frequency wave excitations and responses of the TLP.

In the following, the complete second-order diffraction theory for general three-dimensional bodies, developed in Part 1, is applied to predict the sum-frequency oscillations and tether forces of a full TLP in regular waves. The equations of motion for the high-frequency motions of the TLP are formulated, taking into account the geometric nonlinearities of the tether system. It is shown that the second-order contributions due to these nonlinearities provide additional forcing functions exciting the second-order motions of the TLP. In order to validate the theoretical predictions, a series of model tests has been performed with small scale models of a single- and four-column TLP. Comparisons are made between analysis and experimental data, from which the applicability of the theory is examined.

2. 2 *Theory*

2. 2. 1 *Equations of motion*

Herein the motions of a TLP in regular waves are considered. The motions may be characterised by the six degrees-of-freedom: surge (Ξ_1), sway (Ξ_2), heave (Ξ_3), roll (Ξ_4), pitch (Ξ_5) and yaw (Ξ_6). In regular waves of frequency ω, the motions of the TLP may be described in the form

$$\Xi_k = Re\left[\xi_k^{(1)} e^{-i\omega t} + \xi_k^{(2)} e^{-i2\omega t}\right] + \bar{\Xi}_k, \quad k = 1, 2, \cdots, 6 \tag{2.1}$$

at time t. The first term in Eq. (2.1) represents the wave-frequency responses due to the first-order wave exciting forces. The second term represents the sum-frequency responses due to the second-order wave exciting forces at twice the wave frequency. The last term represents the mean responses due to the wave drift and will not be considered here.

The equations of motion of the TLP may be derived by adding the effects of the tether system to the well-known equations of motion for a freely-floating structure. Omitting the detail of derivation, this leads to the equations of motion

$$\sum_{j=1}^{6}\left[-\omega^2(m_{kj} + M_{kj}^{(1)}) - i\omega N_{kj}^{(1)} - \frac{8}{3\pi} i\omega^2 \hat{N}_{kj}^{(1)} |\xi_j^{(1)}| + K_{kj} + L_{kj}\right] \xi_j^{(1)} = f_{kW}^{(1)}, \quad k = 1, 2, \cdots, 6 \tag{2.2}$$

for the first-order wave-frequency motions, and

$$\sum_{j=1}^{6}\left[-4\omega^2(m_{kj}+M_{kj}^{(2)})-i2\omega N_{kj}^{(2)}-\frac{8}{3\pi}i4\omega^2\hat{N}_{kj}^{(2)}|\xi_j^{(2)}|\right.$$
$$\left.+K_{kj}+L_{kj}\right]\xi_j^{(2)}=f_{kW}^{(2)}+g_{kW}^{(2)},\quad k=1,2,\cdots,6 \tag{2.3}$$

for the second-order sum-frequency motions. In Eqs. (2.2) and (2.3), m_{kj} are the inertia coefficients, $M_{kj}^{(1)}$, $M_{kj}^{(2)}$ are the (frequency-dependent) added inertia coefficients, $N_{kj}^{(1)}$, $N_{kj}^{(2)}$ are the linear (frequency-dependent) added damping coefficients, $\hat{N}_{kj}^{(1)}$, $\hat{N}_{kj}^{(2)}$ are the nonlinear viscous damping coefficients, K_{kj} are the hydrostatic stiffness coefficients, L_{kj} are the mooring stiffness coefficients, $f_{kW}^{(1)}$, $f_{kW}^{(2)}$ are the first- and second-order wave exciting forces, and $g_{kW}^{(2)}$ are the second-order forcing functions exerted by the tether system.

The frequency-dependent added inertia and damping coefficients, and the first-order wave exciting forces may be obtained from conventional first-order diffraction-radiation computations. The method to calculate the second-order sum-frequency wave exciting forces has been elaborated in Part 1 and will not be repeated here. The remainder of this section describes how the terms in Eqs. (2.2) and (2.3) depending on the tether system may be derived.

2. 2. 2 Effects of tether system

a) Assumptions

Consider a floating body anchored to the seabed by N vertical tethers of the lengths l_m, the extensional rigidities k_m and the initial tensions T_{0m} ($m = 1,2,...,N$), as shown in Fig. 2.1. It is assumed that the tethers are massless and that the effects of hydrodynamic forces acting on the tethers are negligible.

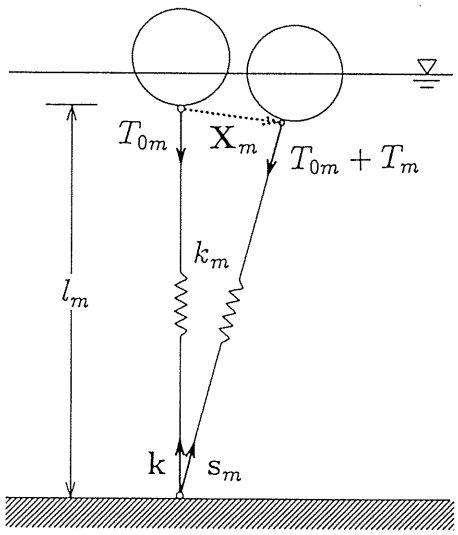

Fig. 2.1 Sketch of tether system.

b) Kinematics of mooring points

The mooring points on the body are denoted by the position vectors x_m relative to the body-fixed co-ordinate axes with an origin at the centre of gravity of the body. The displacement vector $\mathbf{X}_m$ of the point x_m, refered to the space-fixed co-ordinate axes, may be expressed as

$$\mathbf{X}_m = X_{1m}\mathbf{i} + X_{2m}\mathbf{j} + X_{3m}\mathbf{k} = \mathbf{U} + (\underline{D} - \underline{I})\mathrm{x}_m \tag{2.4}$$

where $\mathbf{i}$, $\mathbf{j}$, $\mathbf{k}$ are the unit vectors in the directions of the space-fixed co-ordinate axes, $\mathbf{U}$ is the displacement vector of the centre of gravity,

$$\underline{D} = \begin{bmatrix} \cos\Xi_5\cos\Xi_6 & -\cos\Xi_5\sin\Xi_6 & \sin\Xi_5 \\ \cos\Xi_4\sin\Xi_6 + \sin\Xi_4\sin\Xi_5\cos\Xi_6 & \cos\Xi_4\cos\Xi_6 - \sin\Xi_4\sin\Xi_5\sin\Xi_6 & -\sin\Xi_4\cos\Xi_5 \\ \sin\Xi_4\sin\Xi_6 - \cos\Xi_4\sin\Xi_5\cos\Xi_6 & \sin\Xi_4\cos\Xi_6 + \cos\Xi_4\sin\Xi_5\sin\Xi_6 & \cos\Xi_4\cos\Xi_5 \end{bmatrix} \tag{2.5}$$

and $\underline{I}$ is the 3×3 unit matrix. Eq. (2.5) implies that roll, pitch and yaw are taken in that order[4].

For the present purpose, it is convenient to use the perturbation expansion

$$\mathbf{X}_m = \varepsilon\mathbf{X}_m^{(1)} + \varepsilon^2\mathbf{X}_m^{(2)} + O(\varepsilon^3) \tag{2.6}$$

where ε is the usual perturbation parameter proportional to the wave steepness. The first- and second-order motion vectors $\mathbf{X}_{\mathrm{m}}^{(1)}$, $\mathbf{X}_{\mathrm{m}}^{(2)}$ of the point x_m may then be written as

$$\mathbf{X}_m^{(1)} = X_{1m}^{(1)}\mathbf{i} + X_{2m}^{(1)}\mathbf{j} + X_{3m}^{(1)}\mathbf{k} = \mathbf{U}^{(1)} + \mathbf{W}^{(1)} \times \mathrm{x}_m \tag{2.7}$$

$$\mathbf{X}_m^{(2)} = X_{1m}^{(2)}\mathbf{i} + X_{2m}^{(2)}\mathbf{j} + X_{3m}^{(2)}\mathbf{k} = \mathbf{U}^{(2)} + \mathbf{W}^{(2)} \times \mathrm{x}_m + \underline{H}^{(2)}\mathrm{x}_m \tag{2.8}$$

where $\mathbf{U}^{(1)}$, $\mathbf{U}^{(2)}$ are the first- and second-order displacement vectors of the centre of gravity, $\mathbf{W}^{(1)}$, $\mathbf{W}^{(2)}$ are the first- and second-order small rotation vectors, and

$$\underline{H}^{(2)} = \begin{bmatrix} -\frac{1}{2}(\Xi_5^{(1)2} + \Xi_6^{(1)2}) & 0 & 0 \\ \Xi_4^{(1)}\Xi_5^{(1)} & -\frac{1}{2}(\Xi_4^{(1)2} + \Xi_6^{(1)2}) & 0 \\ \Xi_4^{(1)}\Xi_6^{(1)} & \Xi_5^{(1)}\Xi_6^{(1)} & -\frac{1}{2}(\Xi_4^{(1)2} + \Xi_5^{(1)2}) \end{bmatrix} \tag{2.9}$$

Eqs. (2.7) and (2.8) give the relations between the displacements of the mooring points and the motions of the body.

c) Tether tensions

The extension e_m and the resulting fluctuation of tether force T_m may be obtained from

$$e_m = |l_m\mathbf{k} + \mathbf{X}_m| - l_m = \sqrt{X_{1m}^2 + X_{2m}^2 + (l_m + X_{3m})^2} - l_m \tag{2.10}$$

$$T_m = k_m e_m \tag{2.11}$$

Introducing Eqs. (2.6) ~ (2.8) into Eq. (2.10) and collecting terms of the lowest powers of ε, it follows that

$$e_m = \varepsilon e_m^{(1)} + \varepsilon^2 e_m^{(2)} + O(\varepsilon^3) \tag{2.12}$$

where

$$e_m^{(1)} = X_{3m}^{(1)}, \quad e_m^{(2)} = X_{3m}^{(2)} + \frac{1}{2l_m}(X_{1m}^{(1)2} + X_{2m}^{(1)2}) \tag{2.13}$$

Hence

$$T_m = \varepsilon T_m^{(1)} + \varepsilon^2 T_m{}^{(2)} + O(\varepsilon^3) \tag{2.14}$$

where

$$T_m^{(1)} = k_m X_{3m}^{(1)}, \quad T_m^{(2)} = k_m \left[X_{3m}^{(2)} + \frac{1}{2l_m}(X_{1m}^{(1)2} + X_{2m}^{(1)2}) \right] \tag{2.15}$$

Eq. (2.15) implies that not only the second-order vertical motions but also the quadratic products of the first-order horizontal motions contribute to the second-order tether forces.

d) Resultant tether forces and moments

The resultant tether forces $\mathbf{G}$ exerted on the body may be obtained from

$$\mathbf{G} = -\sum_{m=1}^{N} (T_{0m} + T_m)\mathbf{s}_m \tag{2.16}$$

where $\mathbf{s}_m$ is the unit vector in the direction of the tether in the displaced position

$$\mathbf{s}_m = \frac{1}{l_m + e_m}(l_m\mathbf{k} + \mathbf{X}_m) \tag{2.17}$$

Introducing Eqs. (2.6) ~ (2.8) and (2.12), (2.13) into Eq. (2.17), it follows that

$$\mathbf{s}_m = \mathbf{k} + \varepsilon\mathbf{s}_m^{(1)} + \varepsilon^2\mathbf{s}_m^{(2)} + O(\varepsilon^3) \tag{2.18}$$

where

$$\mathbf{s}_m^{(1)} = \frac{X_{1m}^{(1)}}{l_m}\mathbf{i} + \frac{X_{2m}^{(1)}}{l_m}\mathbf{j} \tag{2.19}$$

$$\mathbf{s}_m^{(2)} = \left(\frac{X_{1m}^{(2)}}{l_m} - \frac{X_{1m}^{(1)}X_{3m}^{(1)}}{l_m^2}\right)\mathbf{i} + \left(\frac{X_{2m}^{(2)}}{l_m} - \frac{X_{2m}^{(1)}X_{3m}^{(1)}}{l_m^2}\right)\mathbf{j} - \frac{X_{1m}^{(1)2} + X_{2m}^{(1)2}}{2l_m^2}\mathbf{k} \tag{2.20}$$

Substituting Eqs. (2.14), (2.15) and (2.18) ~ (2.20) into Eq. (2.17), and collecting powers of ε, the expressions for $\mathbf{G}$ may be derived in the form

$$\mathbf{G} = \mathbf{G}^{(0)} + \varepsilon\mathbf{G}^{(1)} + \varepsilon^2\mathbf{G}^{(2)} + O(\varepsilon^3) \tag{2.21}$$

where

$$\mathbf{G}^{(0)} = -\sum_{m=1}^{N} T_{0m}\mathbf{k} \tag{2.22}$$

$$\mathbf{G}^{(1)} = -\sum_{m=1}^{N}\left(\frac{T_{0m}}{l_m}X_{1m}^{(1)}\mathbf{i} + \frac{T_{0m}}{l_m}X_{2m}^{(1)}\mathbf{j} + k_m X_{3m}^{(1)}\mathbf{k}\right) \tag{2.23}$$

$$\begin{aligned}\mathbf{G}^{(2)} = &-\sum_{m=1}^{N}\left(\frac{T_{0m}}{l_m}X_{1m}^{(2)}\mathbf{i} + \frac{T_{0m}}{l_m}X_{2m}^{(2)}\mathbf{j} + k_m X_{3m}^{(2)}\mathbf{k}\right)\\ &-\sum_{m=1}^{N}\frac{1}{l_m}\left(k_m - \frac{T_{0m}}{l_m}\right)\left[X_{1m}^{(1)}X_{3m}^{(1)}\mathbf{i} + X_{2m}^{(1)}X_{3m}^{(1)}\mathbf{j}\right.\\ &\left.+\frac{1}{2}\left(X_{1m}^{(1)2} + X_{2m}^{(1)2}\right)\mathbf{k}\right]\end{aligned} \tag{2.24}$$

A similar approach may be used to derive the corresponding expressions for the resulting moments $\mathbf{Q}$ of the tether forces on the body. These moments are obtained from

$$\mathbf{Q} = -\sum_{m=1}^{N}(\underline{D}\mathrm{x}_m) \times [(T_{0m} + T_m)\mathbf{s}_m] \tag{2.25}$$

In Eq. (2.25), $\underline{D}\mathrm{x}_m$ represents the displaced position vector of the mooring point x_m, refered to the co-ordinate axes parallel to the space-fixed co-ordinate axes but with an origin at the centre of gravity. Using Eqs. (2.4) and (2.6) ~ (2.8), $\underline{D}\mathrm{x}_m$ may be written as

$$\underline{D}\mathrm{x}_m = \mathrm{x}_m + \varepsilon\left(\mathbf{W}^{(1)} \times \mathrm{x}_m\right) + \varepsilon^2\left(\mathbf{W}^{(2)} \times \mathrm{x}_m + \underline{H}^{(2)}\mathrm{x}_m\right) + O(\varepsilon^3) \tag{2.26}$$

Substituting Eqs. (2.14), (2.15), (2.18) ~ (2.20) and (2.26) into Eq. (2.25), the final expressions for $\mathbf{Q}$ may be derived in the form

$$\mathbf{Q} = \mathbf{Q}^{(0)} + \varepsilon\mathbf{Q}^{(1)} + \varepsilon^2\mathbf{Q}^{(2)} + O(\varepsilon^3) \tag{2.27}$$

where

$$\mathbf{Q}^{(0)} = -\sum_{m=1}^{N} \mathrm{x}_m \times T_{0m}\mathbf{k} \tag{2.28}$$

$$\mathbf{Q}^{(1)} = -\sum_{m=1}^{N} \left[\mathrm{x}_m \times \left(\frac{T_{0m}}{l_m} X_{1m}^{(1)}\mathbf{i} + \frac{T_{0m}}{l_m} X_{2m}^{(1)}\mathbf{j} + k_m X_{3m}^{(1)}\mathbf{k}\right) + \mathbf{W}^{(1)} \times \mathrm{x}_m \times T_{0m}\mathbf{k}\right] \tag{2.29}$$

$$\mathbf{Q}^{(2)} = -\sum_{m=1}^{N} \left[\mathrm{x}_m \times \left(\frac{T_{0m}}{l_m} X_{1m}^{(2)}\mathbf{i} + \frac{T_{0m}}{l_m} X_{2m}^{(2)}\mathbf{j} + k_m X_{3m}^{(2)}\mathbf{k}\right) + \mathbf{W}^{(2)} \times \mathrm{x}_m \times T_{0m}\mathbf{k}\right] - \sum_{m=1}^{N} \left\{\frac{1}{l_m}\left(k_m - \frac{T_{0m}}{l_m}\right)\mathrm{x}_m \times \left[X_{1m}^{(1)} X_{3m}^{(1)}\mathbf{i} + X_{2m}^{(1)} X_{3m}^{(1)}\mathbf{j} + \frac{1}{2}\left(X_{1m}^{(1)2} + X_{2m}^{(1)2}\right)\mathbf{k}\right] + \mathbf{W}^{(1)} \times \mathrm{x}_m \times \left(\frac{T_{0m}}{l_m} X_{1m}^{(1)}\mathbf{i} + \frac{T_{0m}}{l_m} X_{2m}^{(1)}\mathbf{j} + k_m X_{3m}^{(1)}\mathbf{k}\right) + \underline{H}^{(2)}\mathrm{x}_m \times T_{0m}\mathbf{k}\right\} \tag{2.30}$$

The expressions for the resultant tether forces and moments obtained above may be combined more conveniently in the form

$$G_k = G_k^{(0)} + \varepsilon G_k^{(1)} + \varepsilon^2 G_k^{(2)} + O(\varepsilon^3), \quad k = 1, 2, \cdots, 6 \tag{2.31}$$

$G_k^{(0)}$ represents the resultant forces and moments due to the initial tensions, which are balanced with the surplus buoyancy. Using Eqs. (2.7) and (2.8), $G_k^{(1)}$ and $G_k^{(2)}$ may be expressed in terms of the motions of the body as

$$G_k^{(1)} = -L_{kj}\Xi_j^{(1)}, \quad G_k^{(2)} = -L_{kj}\Xi_j^{(2)} + G_{kW}^{(2)} \tag{2.32}$$

where $G_{kW}^{(2)}$ represents the terms consisting of the quadratic products of the first-order body motions. $-L_{kj}\Xi_j^{(n)}$ in Eq. (2.32) correspond to the static restoring forces due to the tether system. $G_{kW}^{(2)}$ provides the additional forcing functions exciting the second-order motions. The equations of motion of a TLP may then be obtained by adding these effects to the well-known equations of motion for a freely-floating structure, as shown in Eqs. (2.2) and (2.3).

2. 3 Experiment

2. 3. 1 Test set-up

To validate the theoretical approach described in the foregoing, a series of model tests has been performed in regular waves with small scale models of a single- and four-column TLP. The principal particulars of the models are presented in Fig. 2.2 and in Table 2.1. Each model made of acrylite was anchored to the tank bottom by four vertical tethers, composed of a combination of stainless wires and steel springs. At the bottom end of each tether, a ring-shaped strain-gauge force transducer was attached to measure the tension in the tether.

On the top of the deck, a white wooden pole was installed on which two black points were marked as the targets to trace the movement of the model by means of a contactless image tracking system. The tests were made in the wave tank at Nagoya Univesity. This facility has a width of 2 m, a nominal water depth of 1 m and a distance of approximately 15 m between the wavemaker and the beach. The models were set up about half way along the length of the tank. The depth of the tank is not large enough to scale the water depth and the tether lengths of the prototype structure. The axial stiffnesses of the tethers were therefore adjusted such that the resonant vertical-plane oscillations due to the springing forces are well excited within the frequency range at which the wavemaker can produce stable waves.

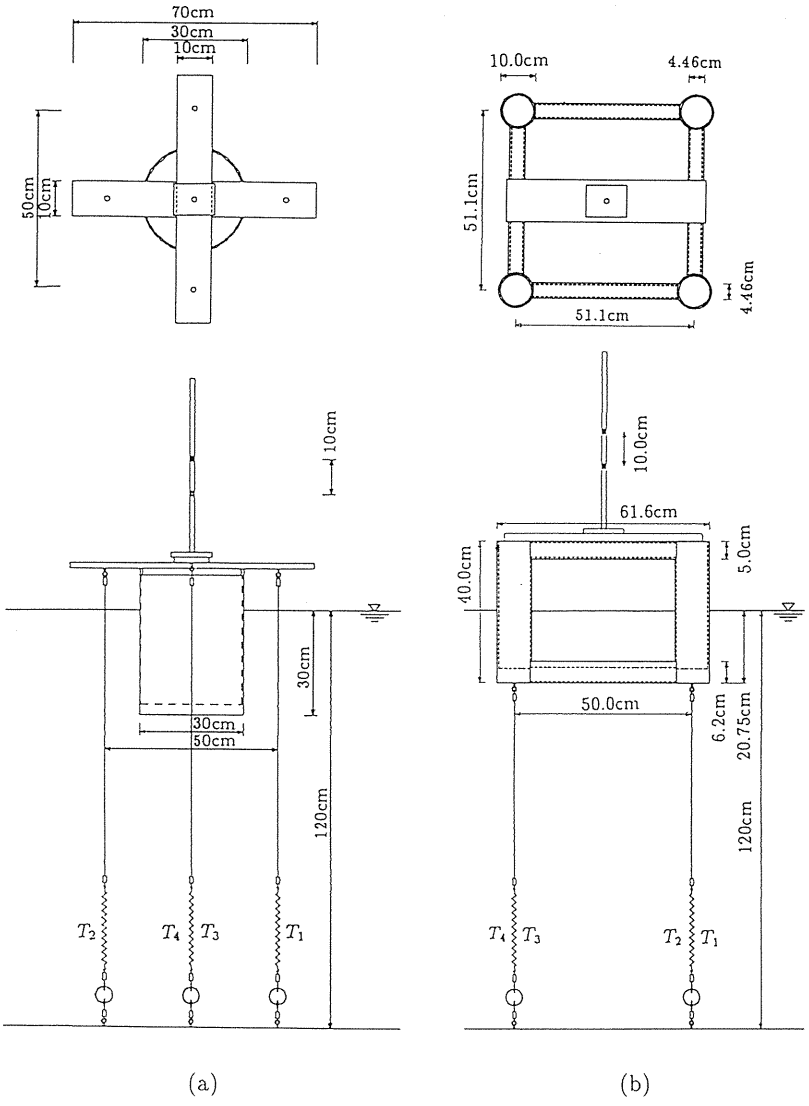

Fig. 2.2 TLP models and test set-up: (a) single-column model, (b) four-column model.

Table 2.1 Principal particulars of TLP models

Description	Value		Unit
	Single-column	Four-column	
Spacing between column centre lines	–	51.1	cm
Column diameter	30	10	cm
Operating draft	30	20.75	cm
Submergence depth of COG	16.724	4.217	cm
Total mass	13219	9495	g
Pitch moment of inertia	3831000	7221700	g·cm^2
Displacement	21206	11351	g
Number of mooring tethers	4	4	–
Length of the tether	125	99.25	cm
Axial stiffness of a tether	889	1011	gf/cm
Pre-tension in a tether	1997	464	gf
Water depth	120	120	cm

2. 3. 2 Generation of waves

Some remarks will be given here on the generation of waves in the wave flume. For the precise measurement of the second-order forces and responses, it is of primary importance to produce the waves correctly to second order. If the wavemaker is controlled by the usual linear control signals, the unfavorable second-order free waves (FWs) are generated by the presence of the wavemaker. Sand and Mansard[27] have suggested that FWs may be eliminated by adding the second-order corrections to the linear control signals. However, it can be shown that this is not necessary if the model is set at some distance from the wave generator. Note that FWs propagate more slowly than the second-order bounded waves (BWs) locked in the first-order waves. (The group velocity of FWs is about half that of BWs in deep water.) When the wave generator is controlled by the linear control signals only, BWs arrive first at the model position, while at that time FWs are still on half way between the wavemaker and the model. Thus, if the experiment is carried out before FWs reach the model, the data without the influence of FWs may be acquired. In this study, this simplified method using the linear control signals only was adopted to avoid the unfavorable effects of the second-order FWs. Fig. 2.3 shows a comparison of the generated second-order incident

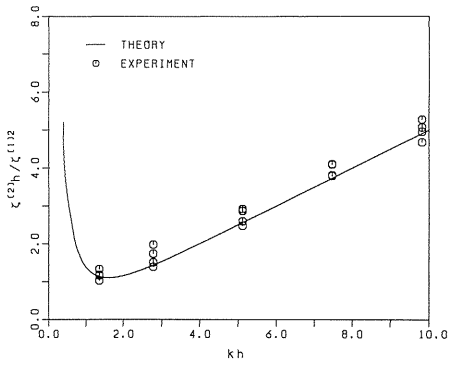

Fig. 2.3 Second-order incident wave amplitude: computed and measured ($\zeta^{(1)}$,$\zeta^{(2)}$=first- and second-order wave amplitudes, k=wave number, h=water depth).

wave amplitudes (normalised with the first-order wave amplitudes squared) with Stokes's second-order wave theory. Agreement is good, confirming the effectiveness of this simplified method to generate waves.

2. 3. 3 Free oscillation tests in still water

Prior to the tests in waves, free oscillation tests were performed in still water to measure the natural frequencies and the dampings for the surge, heave and pitch modes. The linear and nonlinear damping coefficients were determined from the ratios between two subsequent amplitudes of oscillations which were best fitted by means of the least square method. For details see Appendix B.

2. 3. 4 Tests in regular waves

The tests were carried out in regular waves for ranges of wave frequencies (0.5 ~ 1.5 Hz) and amplitudes (1.5 ~ 5 cm). The following quantities were measured:

- Motion responses of moored TLP models by means of a contactless image tracking system.
- Tether forces of moored TLP models by means of ring-shaped strain-guage force transducers.
- Incident wave height by means of a servo-type wave prove positioned 2.5 m in front of the model.

The signals recorded by a cassette-type data recording system were converted to digital data by means of a A-D converter. A harmonic analysis based on the Fast Fourier Transform algorithm was performed to filter out the first and second harmonic components of waves, forces and responses.

2. 4 Discussion of Results

2. 4. 1 Natural frequencies and dampings

The surge, heave and pitch natural frequencies and the corresponding damping coefficients for the four-column TLP, measured from free oscillation tests in still water, are presented in Table 2.2. These damping values were used to predict the motions and tether forces of the model. Free oscillation tests were performed only for the four-column model. For the single column TLP only the potential dampings obtained from the wave diffraction-radiation calculations were used to compute the motions and tether forces.

Table 2. 2 Measured natural frequencies and damping coefficients for four-column TLP model

Mode	Natural frequency	Damping coefficient	
		Linear	Nonlinear
Surge	0.175 Hz	0.6076 gf·s/cm	0.8125 gf·s^2/cm^2
Heave	2.494 Hz	5.2515 gf·s/cm	4.2198 gf·s^2/cm^2
Pitch	2.394 Hz	962.50 gf·cm·s	154440 gf·s^2/cm

2. 4. 2 Motion responses and tether forces

The measured motion responses and tether forces of the TLP models were compared with the theoretical calculations based on the second-order wave diffraction theory. The frequency-dependent added inertia and damping coefficients, and the first- and second-order wave exciting forces on the TLP models were computed using the wave diffraction-radiation code based on the hybrid integral-equation method[18]. Figs. 2.4 to 2.9 show the comparison for the heave and pitch responses and the tether forces of the single-column TLP. It is observed that while the first harmonic components show relatively moderate variations with the wave frequency, the second harmonic components exhibit sharp peaks at the frequencies of 1.18 Hz and 1.26 Hz. The fact that these frequencies coincide with half the heave (2.36 Hz) and pitch (2.56 Hz) natural frequencies of the model suggests the occurence of the resonant oscillations excited by the springing forces at twice the wave frequency. Similar tendencies are also observed in the response curves for the four-column TLP model shown in Figs. 2.10 to 2.14, where the second harmonic components take peak values at the frequencies that coincide with half the pitch (2.39 Hz) and heave (2.49 Hz) natural frequencies of the model. Figs. 2.15 and 2.16 illustrate the examples of measured time histories of response and tether tensions near the resonant frequencies. The existence of significant second harmonic components are clearly observed, which are comparable in magnitude with the first-harmonic wave-frequency responses. Except in the vicinity of the resonant frequencies, the computed results are found to correlate well with the experimental data. However, the large discrepancies observed near the resonant frequencies suggest the need for improved estimates of the damping forces (including mechanical and hydrodynamic).

In order to investigate the influence of the damping values on the motion and tether force predictions, Figs. 2.17 to 2.21 show the comparison of the results computed with measured damping values and those with potential dampings only. Except in the vicinity of the resonant frequencies, the effects of the viscous dampings are found to be negligible. This implies that in these frequencies the accuracy of prediction of the responses depends almost on that of the wave exciting forces. The excellent agreement between theoretical and experimental predictions in these frequencies illustrates the validity of the method to predict the second-order wave exciting forces, described in Part 1.

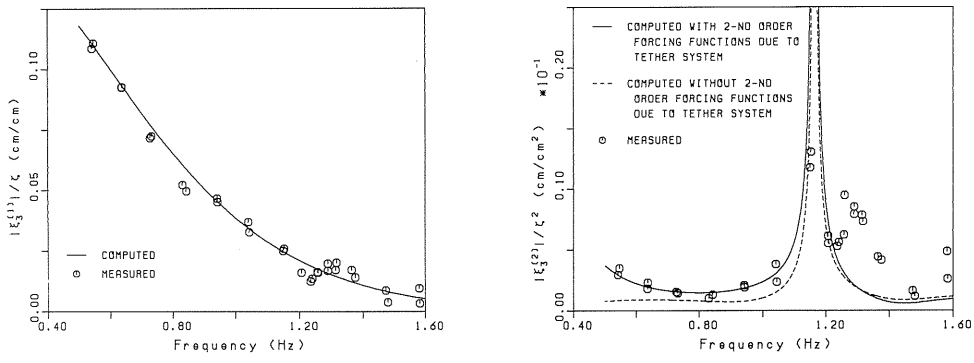

(a) (b)

Fig. 2.4 Comparison between computed and measured heave response of single-column TLP: (a) first harmonic amplitude, (b) second harmonic amplitude.

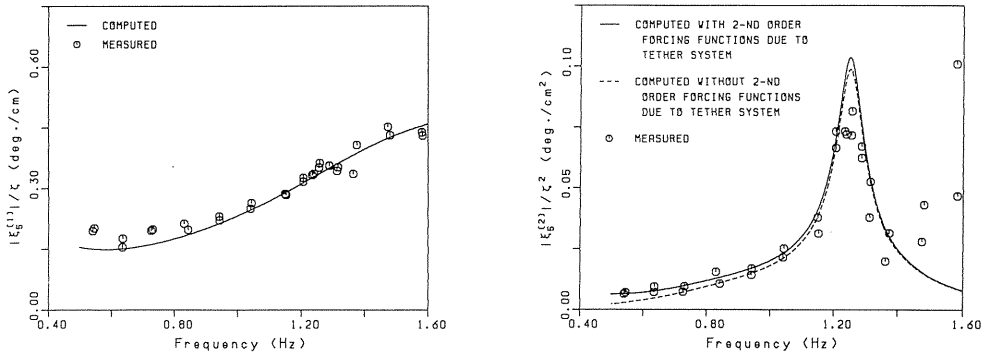

Fig. 2.5 Comparison between computed and measured pitch response of single-column TLP: (a) first harmonic amplitude, (b) second harmonic amplitude.

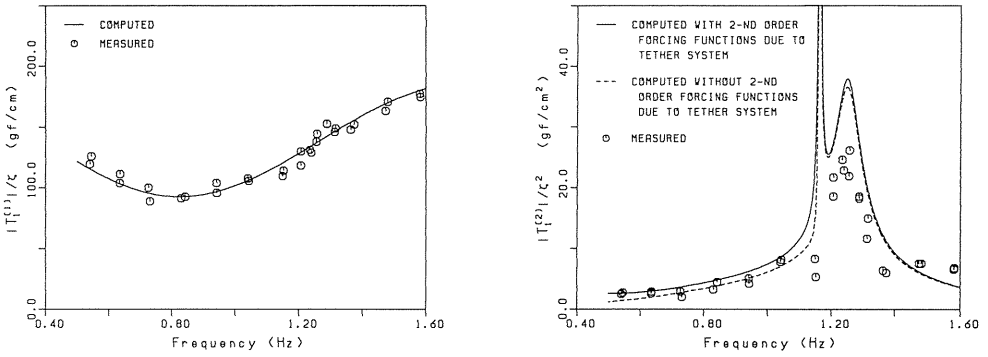

Fig. 2.6 Comparison between computed and measured fore tether force T_1 of single-column TLP: (a) first harmonic amplitude, (b) second harmonic amplitude.

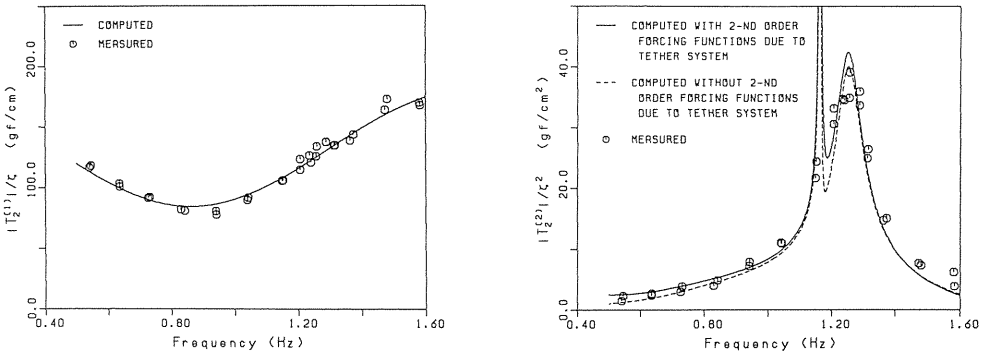

Fig. 2.7 Comparison between computed and measured aft tether force T_2 of single-column TLP: (a) first harmonic amplitude, (b) second harmonic amplitude.

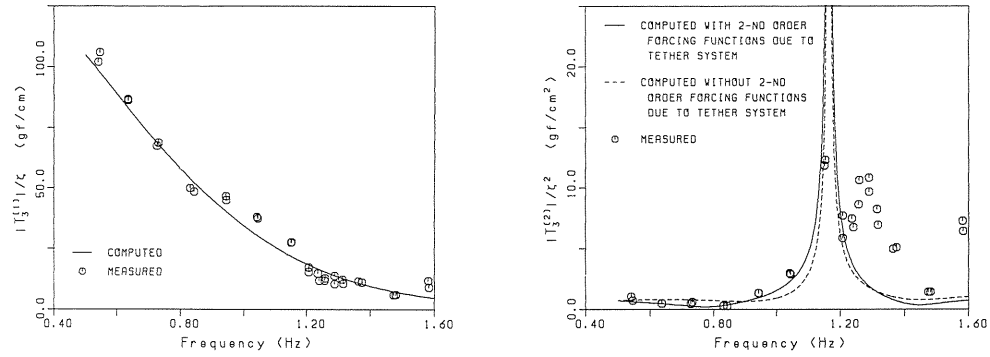

(a) (b)

Fig. 2.8 Comparison between computed and measured mid tether force T_3 of single-column TLP: (a) first harmonic amplitude, (b) second harmonic amplitude.

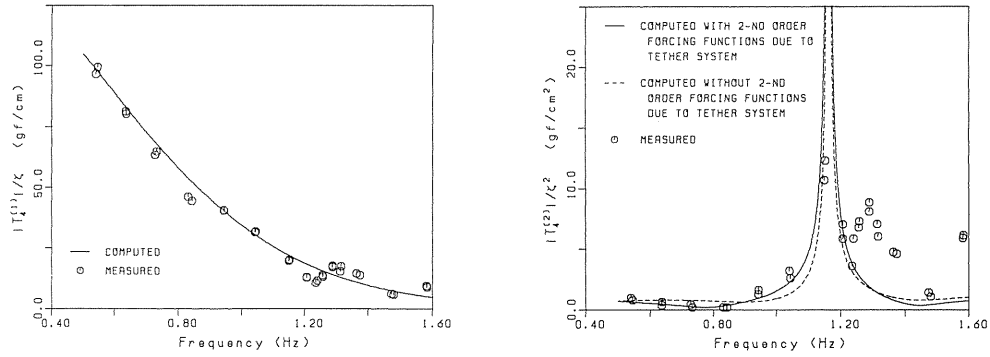

(a) (b)

Fig. 2.9 Comparison between computed and measured mid tether force T_4 of single-column TLP: (a) first harmonic amplitude, (b) second harmonic amplitude.

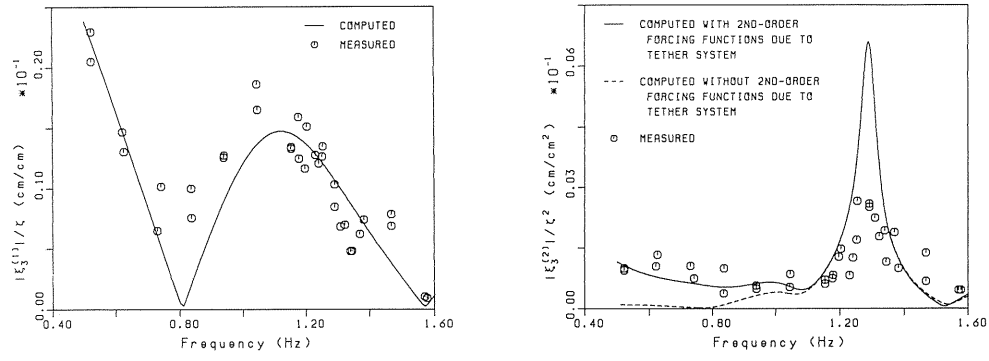

(a) (b)

Fig. 2.10 Comparison between computed and measured heave response of four-column TLP in head waves: (a) first harmonic amplitude, (b) second harmonic amplitude.

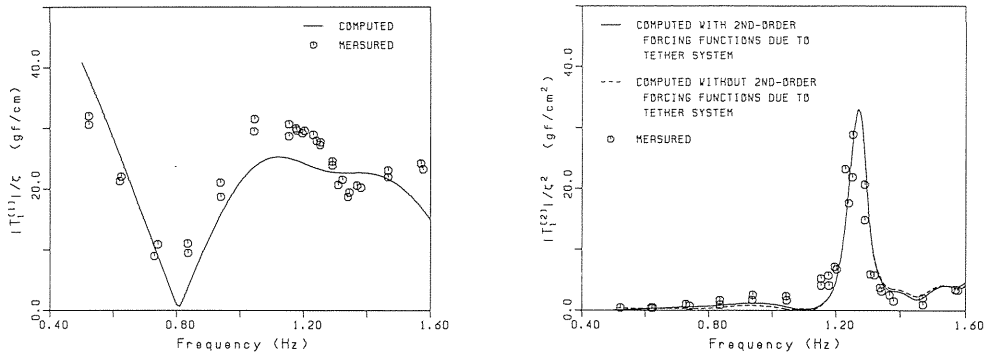

Fig. 2.11 Comparison between computed and measured fore tether force T_1 of four-column TLP in head waves: (a) first harmonic amplitude, (b) second harmonic amplitude.

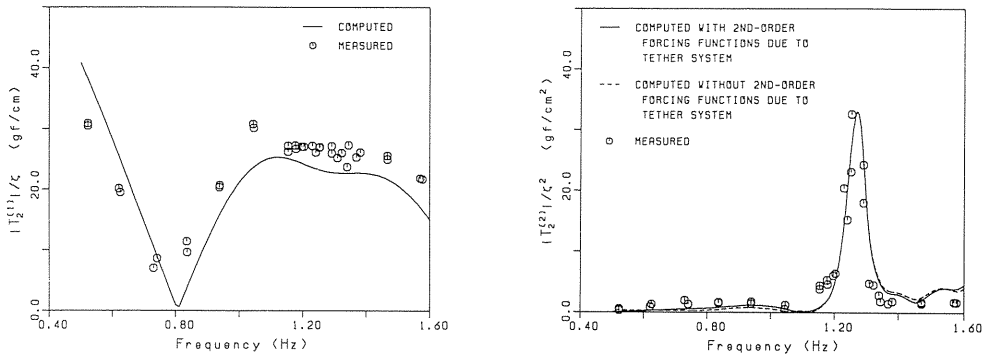

Fig. 2.12 Comparison between computed and measured fore tether force T_2 of four-column TLP in head waves: (a) first harmonic amplitude, (b) second harmonic amplitude.

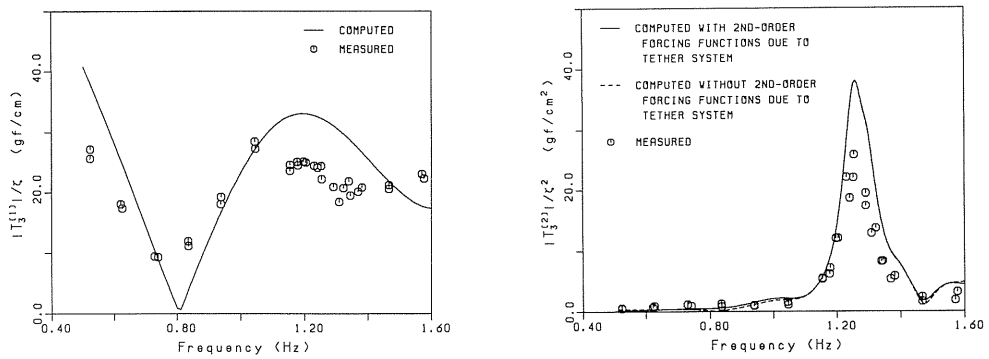

Fig. 2.13 Comparison between computed and measured aft tether force T_3 of four-column TLP in head waves: (a) first harmonic amplitude, (b) second harmonic amplitude.

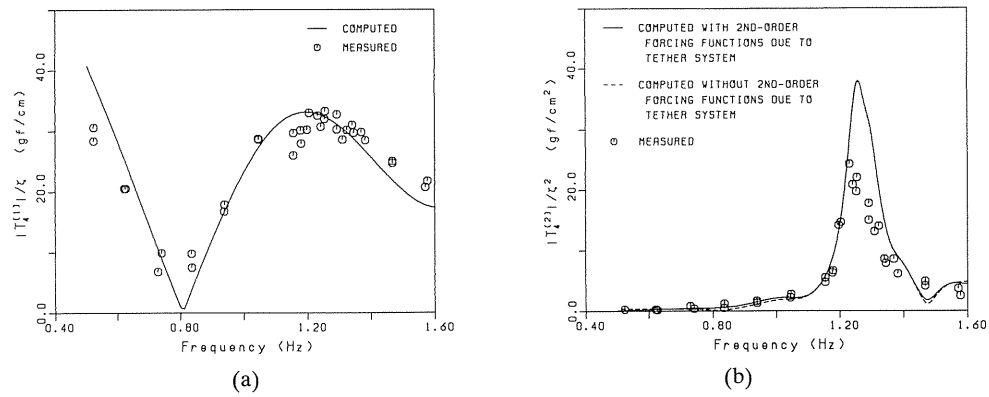

Fig. 2.14 Comparison between computed and measured aft tether force T_4 of four-column TLP in head waves: (a) first harmonic amplitude, (b) second harmonic amplitude.

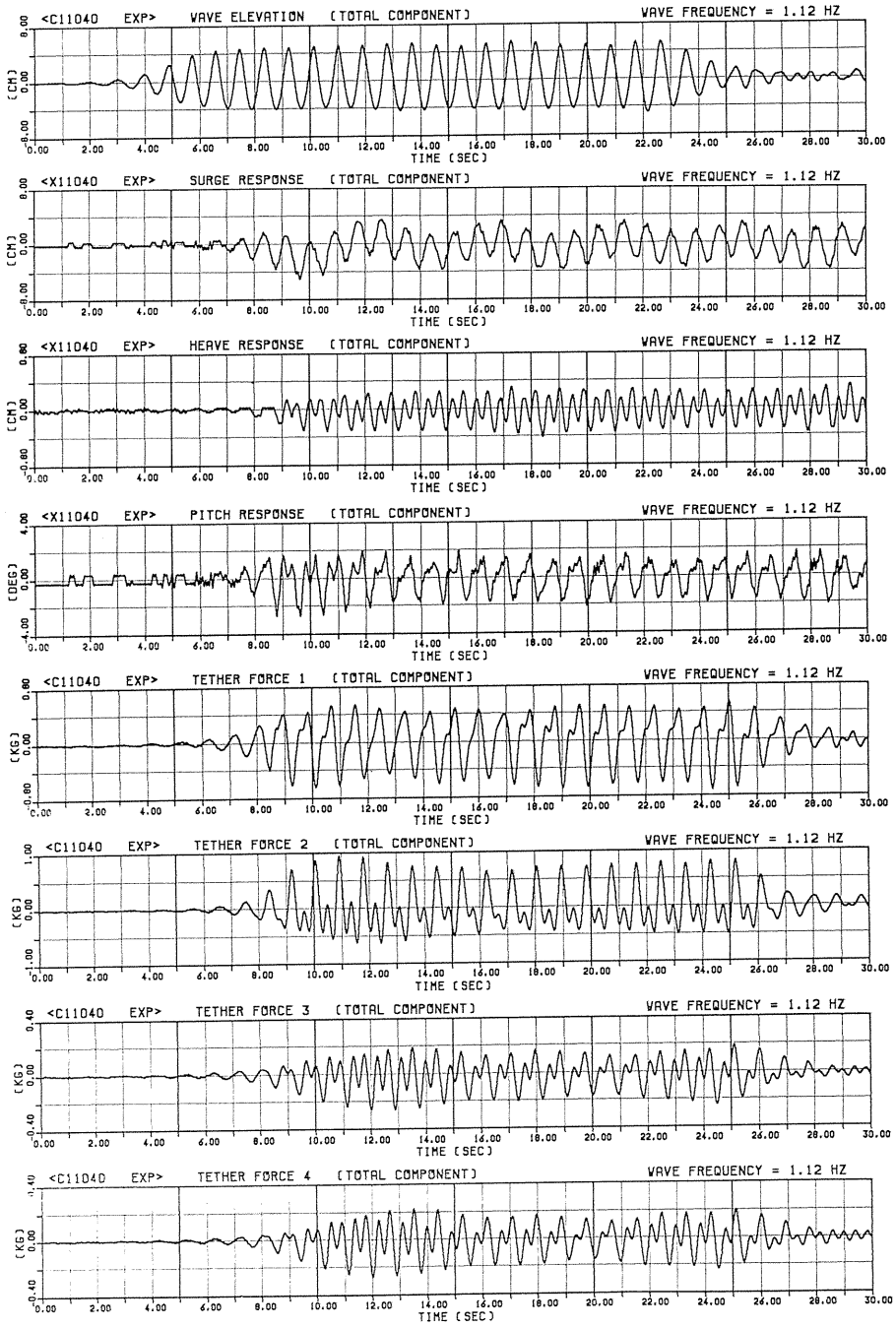

Fig. 2.15 Measured time histories of responses and tether forces of single-column TLP (frequency=1.12 Hz, wave amplitude=4 cm).

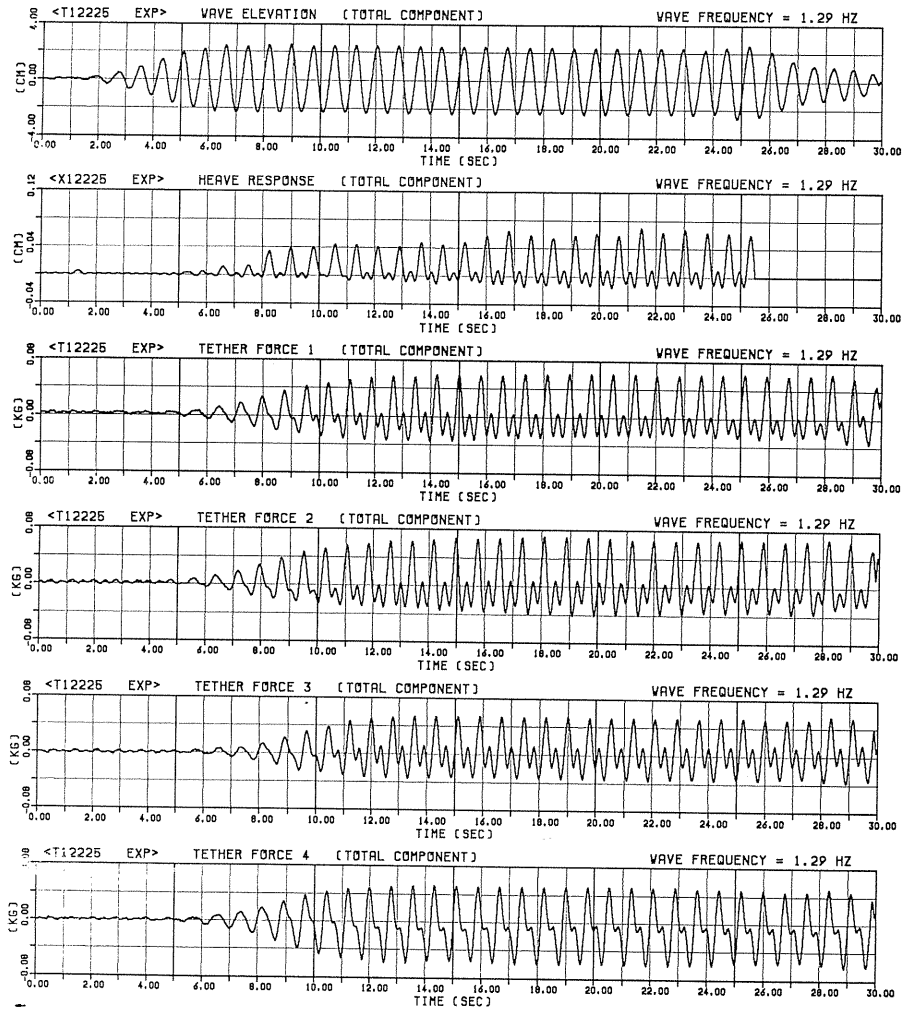

Fig. 2.16 Measured time histories of responses and tether forces of four-column TLP in head waves (frequency=1.29 Hz, wave amplitude=2.35 cm).

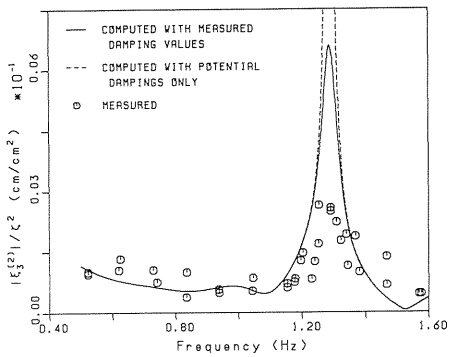

Fig. 2.17 Second harmonic component of heave response of four-column TLP in head waves. Effects of viscous damping forces.

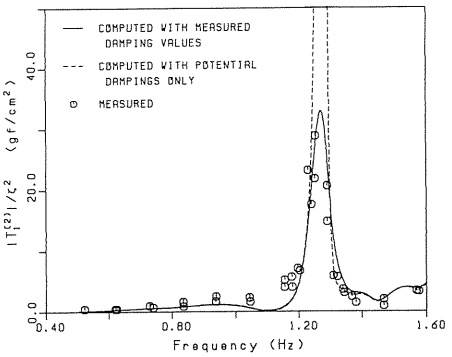

Fig. 2.18 Second harmonic component of fore tether force T_1 of four-column TLP in head waves. Effects of viscous damping forces.

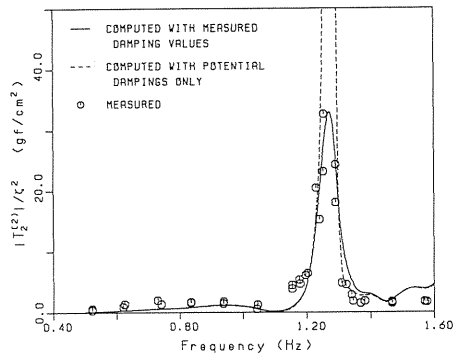

Fig. 2.19 Second harmonic component of fore tether force T_2 of four-column TLP in head waves. Effects of viscous damping forces.

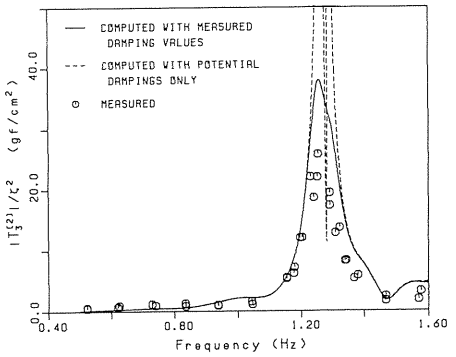

Fig. 2.20 Second harmonic component of aft tether force T_3 of four-column TLP in head waves. Effects of viscous damping forces.

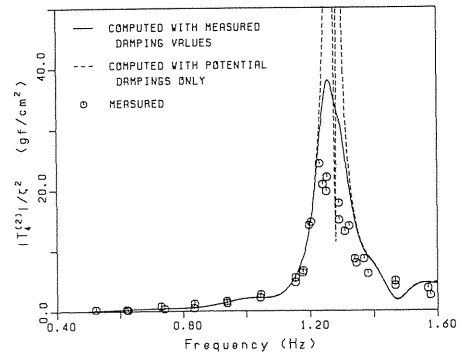

Fig. 2.21 Second harmonic component of aft tether force T_4 of four-column TLP in head waves. Effects of viscous damping forces.

The effects of the additional second-order forcing functions due to the tether system were also investigated as shown in Figs. 2.5 to 2.14. It is observed that these effects are quite significant on the heave response at low frequencies. This is due to large horizontal vessel motions at these frequencies and relatively shallow water depth considered here (see Eq. (2.24)). However, the effects on the tether forces are found to be so small.

2. 5 Conclusions

A series of model tests has been conducted in regular waves to measure the second-order sum-frequency oscillations and tether forces of TLPs. These test results were compared with the predictions based on the complete second-order diffraction theory developed in Part 1. Satisfactory agreement was observed between analysis and experimental data, confirming the validity of the theoretical predictions. The conclusions arising from the present study are summarised as follow:

- The vertical-plane motions and resulting tether forces of the TLPs include the second-order sum-frequency resonant components, which are comparable in magnitude with the first-order wave-frequency responses.
- The nonlinear sum-frequency wave exciting forces, often called 'springing' forces, provide an important source of excitation of such resonant oscillations. These excitation forces can be predicted well based on the second-order wave diffraction theory.
- The theoretical approach described in this paper provides an effective means for predicting the vertical-plane oscillations and tether forces of TLPs, although further researches are needed for better estimates of the damping forces.

Finally, it should be remarked that, due to the size limitation of the wave tank available, the tethering condition studied here may not be realistic. (The water depth is relatively shallow and the tether stiffnesses are relatively low compared with a typical design of TLP.) At the present it is not definite whether the same conclusions are derived for more realistic tethering conditions. This is a matter of future investigation.

Acknowledgement

The author is very grateful to his co-workers, Mr. Tatsuto Suzuki of Nippon Steel Corporation, Mr. Yuhji Sakoh of Kajima Corporation and Mr. Tsuyoshi Nozu of Shimizu Corporation for their collaborations. Sincere thanks are due to Mr. Kimitaka Nozaki, Technical Officer of Department of Architecture, for his continuous help in carrying out this work.

References

1) Matsui, T., Suzuki, T., and Sakoh, Y. "Second-Order Diffraction Forces on Floating Three-Dimensional Bodies in Regular Waves," *Int. J. Offshore and Polar Eng.*, ISOPE, Vol.2, No.3., pp.175–185, 1992.
2) Matsui, T. and Sakoh, Y. "Second-Order Biharmonic Response of a Tension-Leg Platform," *J. Soc. Naval Arch. Japan*, Vol.169, pp.151–164, 1991.

3) Matsui, T., Sakoh, Y. and Nozu, T. "Experimental Measurement of Second-Order Sum-Frequency Oscillations of a Tension-Leg Platform," *Proc. 6th Int. Conf. Behaviour of Offshore Struct.*, London, Vol.1, pp.584–598, 1992.
4) Ogilvie, T.F. "Second-Order Hydrodynamic Effects on Ocean Platforms," *Int. Workshop on Ship and Platform Motions*, Berkeley, pp.205–265, 1983.
5) Hunt, J.N. and Baddour, R.E. "The Diffraction of Nonlinear Progressive Waves by a Vertical Cylinder," *Quarterly J. Mech. and App. Math.*, Vol.34, pp.69–87, 1981.
6) Kim, M.H. and Yue, D.K.P. "The Complete Second-Order Diffraction Solution for an Axisymmetric Body: Part 1. Monochromatic Incident Waves," *J. Fluid Mech.*, Vol.200, pp.235–264, 1989.
7) Kim, M.H. and Yue, D.K.P. "The Complete Second-Order Diffraction Solution for an Axisymmetric Body: Part 2. Bichromatic Incident Waves and Body Motions," *J. Fluid Mech.*, Vol.211, pp.557–593, 1990.
8) Lighthill, M.J. "Waves and Hydrodynamic Loading," *Proc. 2nd Int. Conf. Behaviour of Offshore Struct.*, London, Vol.1, pp.1– 40, 1979.
9) Molin, B. "Second Order Diffraction Loads upon Three Dimensional Bodies," *App. Ocean Res.*, Vol.1, pp.197–202, 1979.
10) Eatock Taylor, R., Hung, S.M. and Chau, F.P. "On the Distribution of Second Order Pressure on a Vertical Cylinder," *App. Ocean Res.*, Vol.11, No.4, pp.183–193, 1989.
11) Eatock Taylor, R. and Hung, S.M. "Second Order Diffraction Forces on a Vertical Cylinder in Regular Waves," *App. Ocean Res.*, Vol.9, No.1, pp.19–30, 1987.
12) Matsui, T. "Slowly Varying Wave Drift Forces on an Articulated Column: 1st Rept. Theory," *J. Soc. Naval Arch. Japan*, Vol.159, pp.149–164, 1986.
13) Matsui, T. "Computation of Slowly Varying Second-Order Hydrodynamic Forces on Floating Structures in Irregular Waves," *J. Offshore Mech. and Arctic Eng.*, Trans. ASME, Vol.111, pp.223–232, 1989.
14) Rahman, M. "Wave Diffraction by Large Offshore Structures: An Exact Second Order Theory," *App. Ocean Res.*, Vol.6, No.2, pp.90–100, 1984.
15) Shimada, K. "Solutions to Three-Dimensional Second-Order Diffraction Problems by Means of Simple-Source Integral-Equation Method," *J. Soc. Naval Arch. Japan*, Vol.161, pp.139–145, 1987.
16) Molin, B. and Marion, A. "Second Order Loads and Motions for Floating Bodies in Regular Waves," *Proc. 5th Int. Offshore Mech. and Arctic Eng. Symp.*, ASME, Tokyo, Vol.1, pp.353–360, 1986.
17) Abramowitz, M. and Stegun, I.A. *Handbook of Mathematical Functions*, 9th ed., Dover, New York, 1982.
18) Matsui, T. and Kato, K. "The Analysis of Wave-Induced Dynamics of Ocean Platforms by Hybrid Integral-Equation Method," *Int. J. Offshore and Polar Eng.*, ISOPE, Vol.1, No.2, pp.146–153, 1991.
19) Ogilvie, T.F. and Tuck, E.O. "A Rational Strip Theory for Ship Motions: Part 1," *Rept. No.013*, Dept. of Naval Architecture and Marine Eng., Univ. of Michigan, 1969.
20) Matsui, T., Ohmori, H., Shirai, T., Endo, M., Sugita, H. and Ohki, K. "Slowly Varying Wave Drift Forces on an Articulated Column: 2nd Rept. Experiment in Regular Waves," *J. Soc. Naval Arch. Japan*, Vol.160, pp.67–76, 1986.
21) Kim, M.H. "Second-Order Sum-Frequency Wave Loads on Large-Volume Structures," *App. Ocean Res.*, Vol.13, No.6, pp.287– 296, 1991.
22) Yoshida, K., Yoneya, T., Oka, N. and Ozaki, M. "Motions and Leg Tensions of Tension Leg Platforms," *Proc. Offshore Tech. Conf.*, OTC4073, Houston, Vol.3, pp.75–87, 1981.
23) Petrauskas, C. and Liu, S.V. "Springing Force Response of a Tension Leg Platform," *Proc. Offshore Tech. Conf.*, OTC5458, Houston, Vol.2, pp.333–341, 1987.
24) De Boom, W.C., Pinkster, J.A. and Tan, S.G. "Motion and Tether Force Prediction for a Deepwater Tension Leg Platform," *Proc. Offshore Tech. Conf.*, OTC4487, Houston, Vol.1, pp.377–388, 1983.

25) Kim, M.H. and Yue, D.K.P. "The Nonlinear Sum-Frequency Wave Excitation and Response of a Tension-Leg Platform," *Proc. 5th Int. Conf. Behaviour of Offshore Struct.*, Trondheim, pp.687–704, 1988.
26) Chau, F.P. "The Second-Order Velocity Potential for Diffraction of Waves by Fixed Offshore Structures," *Ph. D. Thesis*, University College London, 1989.
27) Sand, S.E. and Mansard, E.P.D. "Reproduction of Higher Harmonics in Irregular Waves," *Ocean Eng.*, Vol.13, No.1, pp.57–83, 1986.
28) Hooft, J.P. *Advanced Dynamics of Marine Structures*, John Wiley & Sons, New York, 1982.

Appendices

A. *Proof of Eq. (1.29)*

Using the well-known formulas of vector analysis, the integrand on the left-hand side of Eq. (1.28) can be written in the form

$$\begin{aligned}\nabla \times (\psi_j \mathbf{x}^{(1)} \times \nabla\phi^{(1)}) \cdot \mathbf{n} &= \left[\nabla\psi_j \times (\mathbf{x}^{(1)} \times \nabla\phi^{(1)}) + \psi_j \nabla \times (\mathbf{x}^{(1)} \times \nabla\phi^{(1)})\right] \cdot \mathbf{n} \\ &= \left[\mathbf{x}^{(1)}(\nabla\psi_j \cdot \nabla\phi^{(1)}) - \nabla\phi^{(1)}(\mathbf{x}^{(1)} \cdot \nabla\psi_j)\right] \cdot \mathbf{n} \\ &\quad + \psi_j\Big[(\nabla\phi^{(1)} \cdot \nabla)\,\mathbf{x}^{(1)} - (\mathbf{x}^{(1)} \cdot \nabla)\nabla\phi^{(1)} \\ &\quad + \mathbf{x}^{(1)}(\nabla \cdot \nabla\phi^{(1)}) - \nabla\phi^{(1)}(\nabla \cdot \mathbf{x}^{(1)})\Big] \cdot \mathbf{n} \qquad \text{(A.1)}\end{aligned}$$

By virtue of the assumption of irrotational and ideal flow, and from Eq. (1.6), it follows that

$$\nabla \cdot \nabla\phi^{(1)} = \nabla^2\phi^{(1)} = 0 \qquad \text{(A.2)}$$

$$\nabla \cdot \mathbf{x}^{(1)} = \nabla \cdot (\mathbf{u}^{(1)} + \mathbf{w}^{(1)} \times \mathbf{x}) = 0 \qquad \text{(A.3)}$$

$$\begin{aligned}(\nabla\phi^{(1)} \cdot \nabla)\mathbf{x}^{(1)} \cdot \mathbf{n} &= (\nabla\phi^{(1)} \cdot \nabla)\,(\mathbf{u}^{(1)} + \mathbf{w}^{(1)} \times \mathbf{x}) \cdot \mathbf{n} \\ &= \mathbf{w}^{(1)} \times (\nabla\phi^{(1)} \cdot \nabla)\,\mathbf{x} \cdot \mathbf{n} \\ &= \mathbf{w}^{(1)} \times \nabla\phi^{(1)} \cdot \mathbf{n} = \mathbf{n} \times \mathbf{w}^{(1)} \cdot \nabla\phi^{(1)} \qquad \text{(A.4)}\end{aligned}$$

Making use of Eqs. (A.2) ~ (A.4), Eq. (A.1) can be reduced to

$$\begin{aligned}\nabla \times (\psi_j \mathbf{x}^{(1)} \times \nabla\phi^{(1)}) \cdot \mathbf{n} &= (\mathbf{x}^{(1)} \cdot \mathbf{n})(\nabla\psi_j \cdot \nabla\phi^{(1)}) \\ &\quad - (\mathbf{x}^{(1)} \cdot \nabla\psi_j)(\mathbf{n} \cdot \nabla\phi^{(1)}) - \psi_j\,(\mathbf{w}^{(1)} \times \mathbf{n}) \cdot \nabla\phi^{(1)} \\ &\quad - \psi_j\Big[(\mathbf{x}^{(1)} \cdot \nabla)\nabla\phi^{(1)}\Big] \cdot \mathbf{n} \qquad \text{(A.5)}\end{aligned}$$

Substitution of Eq. (A.5) into Eq. (1.28) leads to Eq. (1.29).

B. Damping Evaluation from Free Oscillation Decay Test

The equation of motion for a single degree-of-freedom system undergoing free oscillation can be described as

$$(m+M)\ddot{y}+N\dot{y}+\hat{N}|\dot{y}|\dot{y}+(K+L)y=0 \tag{B.1}$$

where m is the inertia coefficient, M is the added inertia coefficient, N is the linear added damping coefficient, $\hat{N}$ is the nonlinear viscous damping coefficient, K is the hydrostatic stiffness coefficient and L is the mooring stiffness coefficient. Let the subsequent amplitudes of oscillation be denoted by $y_1, y_2, \cdots, y_{n-1}, y_n, y_{n+1}, \cdots$. The ratio of two subsequent amplitudes can then be expressed as[28)]

$$\frac{y_{n+2}+y_{n+1}}{y_{n+1}+y_n}=\exp\left[-\frac{\pi N}{2(m+M)}\right]\left[1-\frac{2\hat{N}}{3(m+M)}(y_n+y_{n+1})\right] \tag{B.2}$$

Eq. (B.2) may be rewritten in the form

$$z_{n+1}-z_n=-\left\{1-\exp\left[-\frac{\pi N}{2(m+M)}\right]\right\}z_n$$
$$-\frac{2}{3}\exp\left[-\frac{\pi N}{2(m+M)}\right]\hat{N}z_n^2 \tag{B.3}$$

where $z_n = y_n + y_{n+1}$. With the known inertia and added inertia coefficients, m and M, the linear and nonlinear damping coefficients, N and $\hat{N}$, can be determined from the curve $z_{n+1} - z_n$ versus z_n, which are best fitted by means of the least square method, as shown in Figs. B.1 ~ B.3.

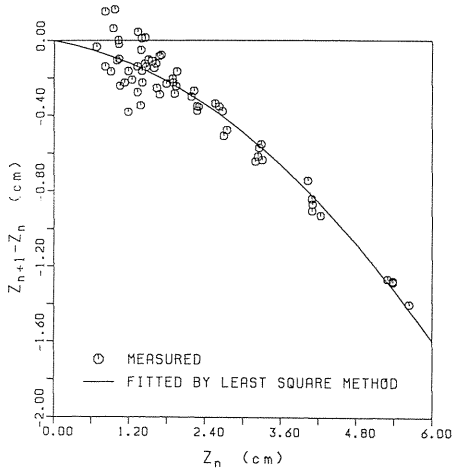

Fig. B.1 Evaluation of surge damping coefficients for four-column TLP by free oscillation decay test.

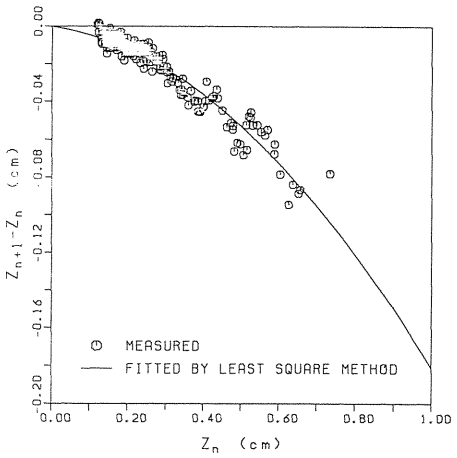

Fig. B.2 Evaluation of heave damping coefficients for four-column TLP by free oscillation decay test.

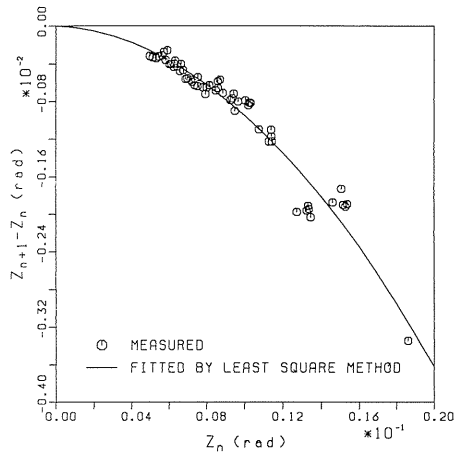

Fig. B.3 Evaluation of pitch damping coefficients for four-column TLP by free oscillation decay test.